

## Non-Oscillatory Hierarchical Reconstruction for Central and Finite Volume Schemes

Yingjie Liu<sup>1,\*</sup>, Chi-Wang Shu<sup>2</sup>, Eitan Tadmor<sup>3</sup> and Mengping Zhang<sup>4</sup>

<sup>1</sup> *School of Mathematics, Georgia Institute of Technology, Atlanta, GA 30332-0160, USA.*

<sup>2</sup> *Division of Applied Mathematics, Brown University, Providence, RI 02912, USA.*

<sup>3</sup> *Department of Mathematics, Institute for Physical Science and Technology, and Center of Scientific Computation and Mathematical Modeling (CSCAMM), University of Maryland, College Park, MD 20742, USA.*

<sup>4</sup> *Department of Mathematics, University of Science and Technology of China, Hefei, Anhui 230026, China.*

Received 30 October 2006; Accepted (in revised version) 11 January 2007

Available online 20 March 2007

---

**Abstract.** This is the continuation of the paper "Central discontinuous Galerkin methods on overlapping cells with a non-oscillatory hierarchical reconstruction" by the same authors. The hierarchical reconstruction introduced therein is applied to central schemes on overlapping cells and to finite volume schemes on non-staggered grids. This takes a new finite volume approach for approximating non-smooth solutions. A critical step for high-order finite volume schemes is to reconstruct a non-oscillatory high degree polynomial approximation in each cell out of nearby cell averages. In the paper this procedure is accomplished in two steps: first to reconstruct a high degree polynomial in each cell by using e.g., a central reconstruction, which is easy to do despite the fact that the reconstructed polynomial could be oscillatory; then to apply the hierarchical reconstruction to remove the spurious oscillations while maintaining the high resolution. All numerical computations for systems of conservation laws are performed without characteristic decomposition. In particular, we demonstrate that this new approach can generate essentially non-oscillatory solutions even for 5th-order schemes without characteristic decomposition.

**AMS subject classifications:** 65M06, 65M60

**Key words:** Central scheme, discontinuous Galerkin method, ENO scheme, finite volume scheme, MUSCL scheme, TVD scheme.

---

\*Corresponding author. *Email addresses:* yingjie@math.gatech.edu (Y. Liu), shu@dam.brown.edu (C.-W. Shu), tadmor@cscamm.umd.edu (E. Tadmor), mpzhang@ustc.edu.cn (M. Zhang)

## 1 Introduction

Finite volume schemes are powerful numerical methods for solving nonlinear conservation laws and related equations. It evolves only cell averages of a solution over time and is locally conservative. The first-order Godunov and Lax-Friedrichs (LxF) schemes are, respectively, the forerunners for the large class of upwind and central high-resolution finite volume schemes. However, the cell average of a solution in a cell contains too little information. In order to obtain higher-order accuracy, neighboring cell averages must be used to reconstruct an approximate polynomial solution in each cell. This reconstruction procedure is the key step for many high-resolution schemes. We mention here the notable examples of the high-resolution upwind FCT, MUSCL, TVD, PPM, ENO, and WENO schemes [6, 11, 13, 14, 26, 42] and this list is far from being complete. The central scheme of Nessyahu and Tadmor (NT) [30] provides a second-order generalization of the staggered LxF scheme. It is based on the same piece-wise linear reconstructions of cell averages used with upwind schemes, yet the solution of (approximate) Riemann problems is avoided. High resolution generalizations of the NT scheme were developed since the 90s as the class of central schemes in e.g. [1, 2, 4, 16, 18, 19, 21, 22, 25, 27, 28, 35] and the list is far from being complete. The second-order MUSCL, high-order ENO and WENO reconstructions are effective non-oscillatory reconstruction methods which select the smoothest possible nearby cell averages to reconstruct the approximate polynomial solution in a cell, and can be used for uniform or unstructured meshes in multi space dimensions. In Hu and Shu [15], WENO schemes for triangular meshes are developed, and in Arminjon and St-Cyr [1], the central scheme with the MUSCL reconstruction is extended to unstructured staggered meshes. When the reconstruction order becomes higher, characteristic decomposition is usually necessary to reduce spurious oscillations for systems of conservation laws. Characteristic decomposition locally creates larger smooth area for polynomial reconstruction by separating discontinuities into different characteristic fields. Comparisons of high-order WENO and central schemes with or without characteristic decomposition are studied in Qiu and Shu [31]. As the formal order of accuracy becomes higher, e.g. 5th-order, spurious oscillations become evident for both schemes without characteristic decomposition (for the Lax problem), even though oscillations in central schemes tend to be smaller.

In a series of works by Cockburn and Shu *et al.* ([8–10] *etc*), discontinuous Galerkin (DG) methods are developed for nonlinear conservation laws and related equations. Compared to finite volume schemes, DG stores and evolves every polynomial coefficient in a cell over time. Therefore there is no need to use information in non-local cells to achieve high-order accuracy. When the solution is non-smooth, similar to finite volume schemes, DG also needs a nonlinear limiting procedure to remove spurious oscillations in order to maintain the high resolution near discontinuities. In Cockburn and Shu [8], a limiting procedure is introduced for DG which compares the variation of the polynomial solution in a cell to the variation of neighboring cell averages to detect the non-smoothness. The nonlinear part of the polynomial is truncated in the non-smooth region.

The limiting procedure is proved to be total variation bounded (TVB). In [5], Biswas, Devine and Flaherty develop a moment limiter which takes into account higher degree terms. In Qiu and Shu [32, 33], the WENO and Hermite WENO reconstructions are developed as limiters for DG. The list of new developments for limiting in DG is growing and is far from being complete. In [29], we develop a central discontinuous Galerkin (DG) method on overlapping cells and a non-oscillatory limiting procedure. The so-called hierarchical reconstruction is related to [5] and to the early work [8]. This limiting procedure requires only linear reconstructions at each stage using information from adjacent cells and can be implemented (at least in theory) for any shape of cells. Therefore it could be useful for unstructured meshes or even for dynamically moving meshes (e.g. Tang and Tang [41]), although we do not pursue too far in unstructured meshes here. Another distinguished feature of the hierarchical reconstruction is that it does not use characteristic decomposition even in high order, which we are going to study further in this work by using the finite volume framework.

We develop a new finite volume approach by using the hierarchical reconstruction introduced in [29]. Instead of directly reconstructing a non-oscillatory polynomial solution in each cell by using the smoothest neighboring cell averages, we break the task into two steps. First we use a central finite volume reconstruction (or other convenient methods) to reconstruct a high degree polynomial in each cell. These polynomials are not necessarily non-oscillatory, therefore the reconstruction can be done in a simple way. Then we apply the hierarchical reconstruction to the piece-wise polynomial solution in order to remove the possible spurious oscillations while keeping the high-order accuracy. With this approach, we demonstrate that both central schemes on overlapping cells and finite volume schemes on non-staggered meshes do not have significant spurious oscillations without characteristic decomposition, for formal order of accuracy as high as 5th-order, although there are still some small overshoots and undershoots at discontinuities of the solution.

This paper is organized as follows. In Section 2, we briefly introduce central schemes on overlapping cells. Finite volume schemes on non-staggered grids are described in Section 3. Various central reconstructions for overlapping cells and non-staggered grids are discussed within these sections. In Section 4, we discuss the non-oscillatory hierarchical reconstruction procedure for these schemes. Numerical examples are presented in Section 5.

## 2 Central schemes on overlapping cells

Consider the scalar one dimensional conservation law

$$\frac{\partial u}{\partial t} + \frac{\partial f(u)}{\partial x} = 0, \quad (x, t) \in \mathcal{R} \times (0, T). \quad (2.1)$$

Set  $\{x_i := x_0 + i\Delta x\}$ , let  $C_{i+1/2} := [x_i, x_{i+1})$  be a uniform partition of  $\mathcal{R}$  and let  $\{\bar{U}_{i+1/2}^n\}$  denote the set of approximate cell averages  $\bar{U}_{i+1/2}^n \approx (1/\Delta x) \int_{C_{i+1/2}} u(x, t^n) dx$ . Similarly,

we set  $D_i := [x_{i-1/2}, x_{i+1/2})$  as the dual partition and let  $\{\bar{V}_i^n\}$  denote the corresponding set of approximate cell average  $\bar{V}_i^n \approx (1/\Delta x) \int_{D_i} u(x, t^n) dx$ . Starting with these two piecewise-constant approximations<sup>†</sup>,

$$\sum_i \bar{U}_{i+1/2}^n \mathbf{1}_{C_{i+1/2}}(x) \quad \text{and} \quad \sum_i \bar{V}_i^n \mathbf{1}_{D_i}(x),$$

we proceed to compute our approximate solution at the next time level,  $t^{n+1} := t^n + \Delta t^n$ . To this end, we reconstruct two higher-order piecewise-polynomial approximations,

$$U^n(x) = \sum_i U_{i+1/2}(x) \mathbf{1}_{C_{i+1/2}}(x) \quad \text{and} \quad V^n(x) = \sum_i V_i(x) \mathbf{1}_{D_i}(x)$$

with breakpoints at  $x_i$ ,  $i = 0, \pm 1, \pm 2, \dots$ , and respectively, at  $x_{i+1/2}$ ,  $i = 0, \pm 1, \pm 2, \dots$ . These piecewise-polynomials should be conservative in the sense that  $\int_{C_{j+1/2}} U^n(x) dx = \Delta x \bar{U}_{j+1/2}^n$  and  $\int_{D_j} V^n(x) dx = \Delta x \bar{V}_j^n$  for all  $j$ 's. Following Nessyahu and Tadmor [30], the central scheme associated with these piecewise-polynomials reads

$$\bar{V}_i^{n+1} = \frac{1}{\Delta x} \int_{D_i} U^n(x) dx - \frac{\Delta t^n}{\Delta x} \left[ f(U^{n+\frac{1}{2}}(x_{i+1/2})) - f(U^{n+\frac{1}{2}}(x_{i-1/2})) \right], \quad (2.2a)$$

$$\bar{U}_{i+1/2}^{n+1} = \frac{1}{\Delta x} \int_{C_{i+1/2}} V^n(x) dx - \frac{\Delta t^n}{\Delta x} \left[ f(V^{n+\frac{1}{2}}(x_{i+1})) - f(V^{n+\frac{1}{2}}(x_i)) \right]. \quad (2.2b)$$

To guarantee second-order accuracy, the right-hand-sides of (2.2a), (2.2b) require the approximate values of  $U^{n+\frac{1}{2}}(x_{j+1/2}) \approx u(x_{j+1/2}, t^{n+\frac{1}{2}})$  and  $V^{n+\frac{1}{2}}(x_j) \approx u(x_j, t^{n+\frac{1}{2}})$  to be evaluated at the midpoint  $t + \Delta t^n/2$ . Replacing the midpoint rule with higher-order quadratures, yields higher-order accuracy, e.g., [4, 27].

The central Nessyahu-Tadmor (NT) scheme (2.2) and its higher-order generalizations provide effective high-resolution "black-box" solvers to a wide variety of nonlinear conservation laws. When  $\Delta t$  is very small, however, e.g., with  $\Delta t = \mathcal{O}((\Delta x)^2)$  as required by the CFL condition for convection-diffusion equations for example, the numerical dissipation of the NT schemes becomes excessively large. The excessive dissipation is due to the staggered grids where at each time-step, cell averages are shifted  $\Delta x/2$ -away from each other. To address this difficulty, Kurganov and Tadmor, [22], suggested to remove this excessive dissipation by using staggered grids which are shifted only  $\mathcal{O}(\Delta t)$ -away from each other. This amounts to using control volumes of width  $\mathcal{O}(\Delta t)$  so that the resulting schemes admits semi-discrete limit as  $\Delta t \rightarrow 0$ , the so called "central-upwind" schemes introduced in [22] and further generalized in [21]. Recent work on reduction of numerical dissipation in central-upwind schemes can be found in [20]. Liu [28] introduced another modification of the NT scheme which removes its  $\mathcal{O}(1/\Delta t)$  dependency of numerical dissipation. In this approach, one takes advantage of the redundant representation of

<sup>†</sup>Here and below,  $\mathbf{1}_\Omega(x)$  denotes the characteristic function of  $\Omega$ .

the solution over overlapping cells,  $\bar{V}_i^n$  and  $\bar{U}_{i+1/2}^n$ . The idea is to use a  $\mathcal{O}(\Delta t)$ -dependent weighted average of  $\bar{U}_{i+1/2}^n$  and  $\bar{V}_i^n$ . To simplify our discussion, we momentarily give up second-order accuracy in time, setting  $U^{n+\frac{1}{2}} = U^n$  and  $V^{n+\frac{1}{2}} = V^n$  in (2.2a) and (2.2b). The resulting first-order forward-Euler formulation of the new central scheme reads

$$\bar{V}_i^{n+1} = \theta \left( \frac{1}{\Delta x} \int_{D_i} U^n(x) dx \right) + (1-\theta) \bar{V}_i^n - \frac{\Delta t^n}{\Delta x} [f(U^n(x_{i+1/2})) - f(U^n(x_{i-1/2}))], \quad (2.3a)$$

$$\bar{U}_{i+1/2}^{n+1} = \theta \left( \frac{1}{\Delta x} \int_{C_{i+1/2}} V^n(x) dx \right) + (1-\theta) \bar{U}_{i+1/2}^n - \frac{\Delta t^n}{\Delta x} [f(V^n(x_{i+1})) - f(V^n(x_i))]. \quad (2.3b)$$

Here  $\theta := \Delta t^n / \Delta \tau^n$  where  $\Delta t^n = t^{n+1} - t^n$  is the time step size,  $\Delta t^n \leq \Delta \tau^n$ ,  $\Delta \tau^n$  is a parameter dictated by the CFL condition. ( $\Delta \tau^n = (\text{CFL factor}) \times \Delta x / (\text{maximum characteristics speed})$ ), where the CFL factor should be less than 1/2. At the time  $t^n$ ,  $\Delta \tau^n$  is first chosen with certain CFL factor, then  $\Delta t^n$  has the freedom to take any value in  $(0, \Delta \tau^n]$  without introducing excessive dissipation. The smaller  $\Delta \tau^n$  is chosen, the larger the numerical dissipation is. We find in numerical experiments that setting  $\Delta \tau^n$  with CFL factor 0.4 is robust. In some numerical tests with less interactions of discontinuities, we can choose larger  $\Delta \tau^n$ .) Note that when  $\theta = 1$ , (2.3a), (2.3b) is reduced to the first-order, forward-Euler-based version of the NT scheme (2.2a), (2.2b). The reduced dissipation allows us to pass to a semi-discrete formulation: subtracting  $\bar{V}_i^n$  and  $\bar{U}_{i+1/2}^n$  from both sides, multiplying by  $\frac{1}{\Delta t^n}$ , and then passing to the limit as  $\Delta t^n \rightarrow 0$  we end up with

$$\begin{aligned} & \frac{d}{dt} \bar{V}_i(t^n) \\ &= \frac{1}{\Delta \tau^n} \left( \frac{1}{\Delta x} \int_{D_i} U^n(x) dx - \bar{V}_i^n \right) - \frac{1}{\Delta x} [f(U^n(x_{i+1/2})) - f(U^n(x_{i-1/2}))], \end{aligned} \quad (2.4a)$$

$$\begin{aligned} & \frac{d}{dt} \bar{U}_{i+1/2}(t^n) \\ &= \frac{1}{\Delta \tau^n} \left( \frac{1}{\Delta x} \int_{C_{i+1/2}} V^n(x) dx - \bar{U}_{i+1/2}^n \right) - \frac{1}{\Delta x} [f(V^n(x_{i+1})) - f(V^n(x_i))]. \end{aligned} \quad (2.4b)$$

The spatial accuracy of the semi-discrete central scheme (2.4) is dictated by the order the reconstruction  $U^n(x)$  and  $V^n(x)$ . The strong stability-preserving (SSP) Runge-Kutta methods [12, 39] yield the matching high-order discretization in time. There are two reconstruction procedures for overlapping cells: one is the standard procedure to reconstruct the two classes of cell averages  $\{\bar{V}_i^n : i=0, \pm 1, \pm 2, \dots\}$  and  $\{\bar{U}_{i+1/2}^n : i=0, \pm 1, \pm 2, \dots\}$ ; the other couples these two classes for reconstruction of the final representation of the solution. Thus, this approach is redundant. At the same time, numerical examples in [28] have shown that by coupling the reconstructions, redundancy does provide improved resolution when compared with the one-cell average evolution approach of Godunov-type schemes.

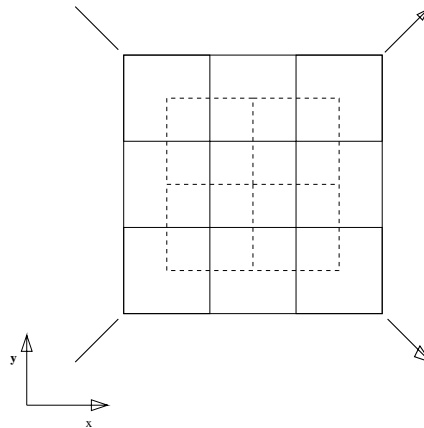


Figure 1: 2D overlapping cells by collapsing the staggered dual cells on two adjacent time levels to one time level.

### 2.1 Extension to multi dimensions

Consider the scalar conservation law

$$\frac{\partial u}{\partial t} + \nabla_{\mathbf{x}} \cdot \mathbf{f}(\mathbf{u}) = 0, \quad (\mathbf{x}, t) \in \mathcal{R}^d \times (0, T), \tag{2.5}$$

where  $\mathbf{u} = (u_1, \dots, u_m)^\top$ . For simplicity, assume a uniform staggered rectangular mesh depicted in figure 1 for the 2D case. Let  $\{C_{I+1/2}\}$ ,  $I = (i_1, i_2, \dots, i_d)$  be a partition of  $\mathcal{R}^d$  into uniform square cells depicted by solid lines in figure 1 and tagged by their cell centroids at the half integers,  $\mathbf{x}_{I+1/2} := (I+1/2)\Delta x$ . Let  $\bar{U}_{I+1/2}(t)$  be the numerical cell average approximating  $(1/|C_{I+1/2}|) \int_{C_{I+1/2}} u(\mathbf{x}, t) d\mathbf{x}$ , in particular,  $\bar{U}_{I+1/2}^n = \bar{U}_{I+1/2}(t^n)$ . Let  $\{D_I\}$  be the dual mesh which consists of a  $\Delta x/2$ - shift of the  $C_{I+1/2}$ 's depicted by dash lines in Fig. 1. Let  $\mathbf{x}_I$  be the cell centroid of the cell  $D_I$ . Let  $\bar{V}_I(t)$  be the numerical cell average approximating  $(1/|D_I|) \int_{D_I} u(\mathbf{x}, t) d\mathbf{x}$ . The semi-discrete central scheme on overlapping cells can be written as follows [28]:

$$\begin{aligned} & \frac{d}{dt} \bar{U}_{I+1/2}(t^n) \\ &= \frac{1}{\Delta \tau^n} \left( \frac{1}{|C_{I+1/2}|} \int_{C_{I+1/2}} V^n(\mathbf{x}) d\mathbf{x} - \bar{U}_{I+1/2}^n \right) - \frac{1}{|C_{I+1/2}|} \int_{\partial C_{I+1/2}} \mathbf{f}(V^n(\mathbf{x})) \cdot \mathbf{n} ds, \end{aligned} \tag{2.6a}$$

$$\begin{aligned} & \frac{d}{dt} \bar{V}_I(t^n) \\ &= \frac{1}{\Delta \tau^n} \left( \frac{1}{|D_I|} \int_{D_I} U^n(\mathbf{x}) d\mathbf{x} - \bar{V}_I^n \right) - \frac{1}{|D_I|} \int_{\partial D_I} \mathbf{f}(U^n(\mathbf{x})) \cdot \mathbf{n} ds. \end{aligned} \tag{2.6b}$$

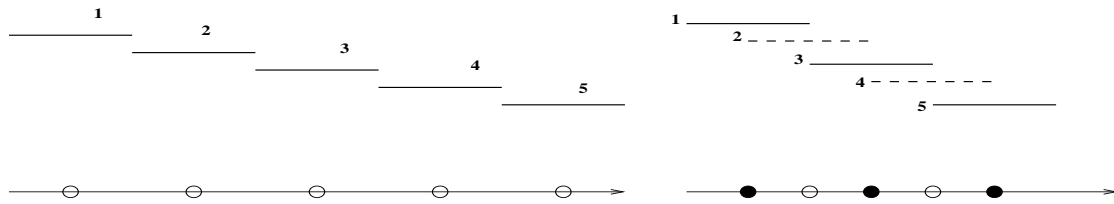


Figure 2: Left: 1D non-staggered cells. Right: 1D overlapping cells. To construct a 4th degree polynomial for cell 3 involves cell 1,2,4,5 and 3.

## 2.2 Central reconstructions

Standard non-oscillatory finite volume reconstruction procedures such as ENO [14, 39] or WENO [17, 26] *etc*, choose the smoothest possible nearby cell averages to construct a non-oscillatory high-order polynomial in a cell. Here we take a different approach: first construct a polynomial of the desired degree (which could be oscillatory) in each cell by using a central finite volume reconstruction (or other finite volume reconstructions); then apply the hierarchical reconstruction ([29], also described in Section 4) to remove the possible spurious oscillations while keeping the formal order of accuracy of the central finite volume reconstruction. For systems of conservation laws, we use a component-wise extension of (2.6) without characteristic decomposition. One of the special properties of this new approach is that we observe essentially non-oscillatory numerical solutions near discontinuities even for 5th-order schemes without characteristic decomposition, though small overshoots do occur. Conventional methods without characteristic decomposition tend to generate more evident artifacts or oscillations beyond 3rd-order formal accuracy, see e.g. [31].

### 2.2.1 Central reconstructions in 1D

For convenience, we use a slightly different notation from previous subsections and assume the approximate cell average  $\bar{U}_i$  is given at the overlapping cell  $C_i$ , with cell center  $x_i$ ,  $i = 1, 2, \dots, 5$ , see Fig. 2 (right). In order to construct a quadratic polynomial  $U_3(x - x_3) = U_3(0) + U_3'(0)(x - x_3) + \frac{1}{2}U_3''(0)(x - x_3)^2$  in cell  $C_3$ , one can solve the linear system

$$\frac{1}{|C_i|} \int_{C_i} U_3(x - x_3) dx = \bar{U}_i, \quad i = 2, 3, 4.$$

Similarly, in order to construct a 4th-degree polynomial  $U_3(x - x_3) = U_3(0) + U_3'(0)(x - x_3) + \frac{1}{2}U_3''(0)(x - x_3)^2 + \frac{1}{3!}U_3^{(3)}(0)(x - x_3)^3 + \frac{1}{4!}U_3^{(4)}(0)(x - x_3)^4$  in cell  $C_3$ , one solves the linear system

$$\frac{1}{|C_i|} \int_{C_i} U_3(x - x_3) dx = \bar{U}_i, \quad i = 1, 2, 3, 4, 5.$$

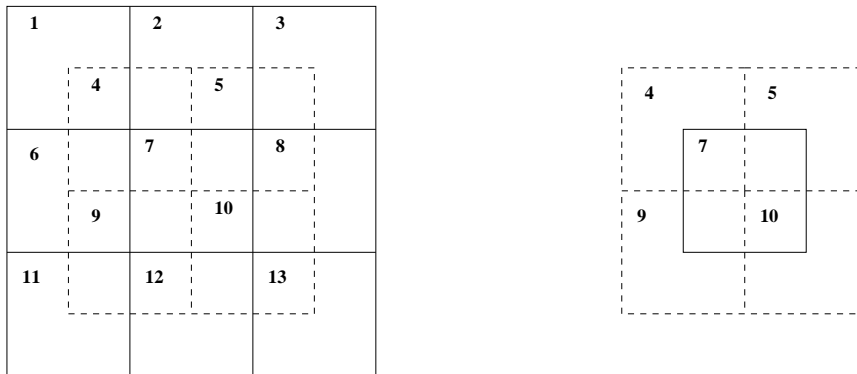


Figure 3: 2D overlapping cells. Left: to construct a cubic polynomial in cell 7 involves cell averages from 13 adjacent overlapping cells. Right: non-oscillatory hierarchical reconstruction for cell 7 involves only polynomials in overlapping cell 4,5,9,10 and 7.

**2.2.2 A central 4th-order reconstruction in 2D**

Assume that the approximate cell average  $\bar{U}_i$  is given at the overlapping cell  $C_i$ , with cell centroid  $\mathbf{x}_i$ ,  $i = 1, 2, \dots, 13$ , see Fig. 3 (left). In order to construct a cubic polynomial  $U_7(\mathbf{x} - \mathbf{x}_7)$  in cell  $C_7$ , we need 10 nearby cell averages. One could certainly pick a suitable set of 10 cells (including cell  $C_7$ ) out of the 13 cells adjacent to cell  $C_7$ . Here we take a more systematic least square approach following [3, 15],

$$\min \left\{ \sum_{1 \leq i \leq 13, i \neq 7} \left[ \frac{1}{|C_i|} \int_{C_i} U_7(\mathbf{x} - \mathbf{x}_7) d\mathbf{x} - \bar{U}_i \right]^2 \right\},$$

subject to

$$\frac{1}{|C_7|} \int_{C_7} U_7(\mathbf{x} - \mathbf{x}_7) d\mathbf{x} = \bar{U}_7.$$

This can be solved by the method of Lagrangian multiplier. Let

$$\mathcal{G} = \sum_{1 \leq i \leq 13, i \neq 7} \left[ \frac{1}{|C_i|} \int_{C_i} U_7(\mathbf{x} - \mathbf{x}_7) d\mathbf{x} - \bar{U}_i \right]^2 + \alpha \left[ \frac{1}{|C_7|} \int_{C_7} U_7(\mathbf{x} - \mathbf{x}_7) d\mathbf{x} - \bar{U}_7 \right].$$

Then  $\nabla \mathcal{G} = 0$  yields a linear system. The coefficient matrix of the linear system is invariant from cell to cell for the uniform mesh. Therefore the least square problem is solved only once and the inverse of the coefficient matrix can be stored for calculating a cubic polynomial in each cell.

We also apply this reconstruction to an irregular staggered mesh such that for one class of cells,  $\Delta x = \Delta y = h$  in the upper half domain and  $\Delta x = 2\Delta y = h$  in the lower half domain .

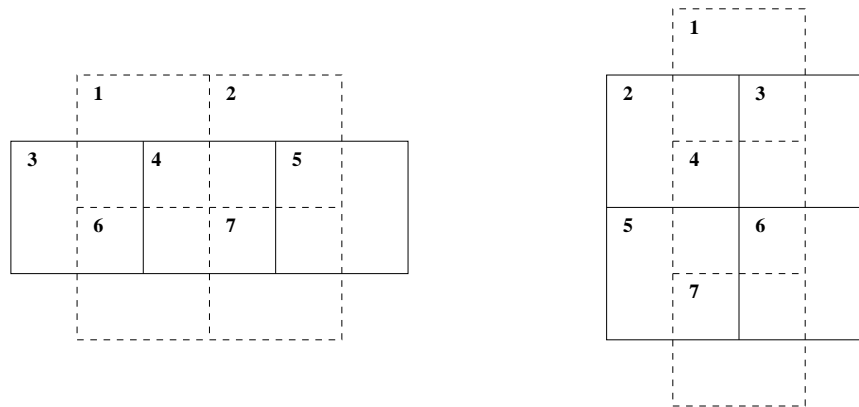


Figure 4: 2D overlapping cells. Left: to construct a quadratic polynomial in cell 4 (belongs to one class) involves cell averages from 7 adjacent overlapping cells. Right: to construct a quadratic polynomial in cell 4 (belongs to the dual class) involves different set of cells.

### 2.2.3 A central 3rd-order reconstruction in 2D

The similar least square strategy can also be used to reconstruct a quadratic polynomial in each cell. However, we want to try a different reconstruction method here. It is non-symmetric and is slightly different for the two classes of overlapping cells, see Fig. 4. On the left, suppose cell  $C_4$  belongs to a cell class of the two overlapping cell classes, we can reconstruct a quadratic polynomial  $U_4(\mathbf{x} - \mathbf{x}_4)$  in cell  $C_4$  by solving

$$\frac{1}{|C_i|} \int_{C_i} U_4(\mathbf{x} - \mathbf{x}_4) d\mathbf{x} = \bar{U}_i, \quad i = 1, 2, 4, 6, 7,$$

and

$$\int_{C_3 \cup C_5} U_4(\mathbf{x} - \mathbf{x}_4) d\mathbf{x} = \bar{U}_3 |C_3| + \bar{U}_5 |C_5|.$$

On the right of Fig. 4, supposing cell  $C_4$  belongs to the dual cell class, we can reconstruct a quadratic polynomial  $U_4(\mathbf{x} - \mathbf{x}_4)$  in cell  $C_4$  by solving

$$\frac{1}{|C_i|} \int_{C_i} U_4(\mathbf{x} - \mathbf{x}_4) d\mathbf{x} = \bar{U}_i, \quad i = 2, 3, 4, 5, 6,$$

and

$$\int_{C_1 \cup C_7} U_4(\mathbf{x} - \mathbf{x}_4) d\mathbf{x} = \bar{U}_1 |C_1| + \bar{U}_7 |C_7|.$$

Even though the reconstruction is non-symmetric for each class of cells, their combination has no preference in each coordinate direction.

## 3 Finite volume schemes

The new finite volume approach can also be applied to non-staggered meshes. We first study a 5th-order finite volume scheme on the 1D uniform grid for equation (2.1). Re-

call that  $\{x_i := x_0 + i\Delta x\}$ ,  $C_{i+1/2} := [x_i, x_{i+1})$  is a uniform partition of  $\mathcal{R}$ , and  $\{\bar{U}_{i+1/2}^n\}$  (or  $\{\bar{U}_{i+1/2}(t^n)\}$ ) denotes the set of approximate cell averages  $\bar{U}_{i+1/2}^n \approx (1/\Delta x) \int_{C_{i+1/2}} u(x, t^n) dx$ . Out of these approximate cell averages, one can apply a conservative finite volume reconstruction to obtain a piece-wise polynomial  $U^n(x)$  (or  $U(x, t^n)$ ) with breaking points at  $\{x_i\}$ . Then the semi-discrete finite volume formulation can be written as follows (see e.g. [38] for more details)

$$\frac{d}{dt} \bar{U}_{i+1/2}(t^n) = -\frac{1}{\Delta x} (\hat{f}_{i+1}^n - \hat{f}_i^n), \quad (3.1)$$

where  $\hat{f}_i^n$  is the numerical flux defined by  $\hat{f}_i^n = h(U^n(x_{i-}), U^n(x_{i+}))$ . Here we use the Lax-Friedrichs (LF) flux:

$$h(a, b) = \frac{1}{2} [f(a) + f(b) - \beta(b - a)],$$

where  $\beta = \max_u |f'(u)|$  is the largest characteristic speed. For systems of conservation laws, we use a component-wise extension of (3.1) without characteristic decomposition.

### 3.1 A 5th-order central reconstruction in 1D

Assume the approximate cell average  $\bar{U}_i$  is given at cell  $C_i$ , with cell center  $x_i$ ,  $i=1, 2, \dots, 5$ , see Fig. 2 (left). In order to construct a 4th degree polynomial  $U_3(x - x_3) = U_3(0) + U_3'(0)(x - x_3) + \frac{1}{2}U_3''(0)(x - x_3)^2 + \frac{1}{3!}U_3^{(3)}(0)(x - x_3)^3 + \frac{1}{4!}U_3^{(4)}(0)(x - x_3)^4$  in cell  $C_3$ , one solves the following linear system

$$\frac{1}{|C_i|} \int_{C_i} U_3(x - x_3) dx = \bar{U}_i, \quad i = 1, 2, 3, 4, 5.$$

The reconstructed polynomial can be oscillatory near discontinuities of the solution. The next step is to apply the hierarchical reconstruction to remove possible spurious oscillations.

### 3.2 A 4th-order central reconstructions in 2D

In Fig. 5 (left), in order to reconstruct a cubic polynomial in cell  $C_7$ , we use a similar method as in Section 2.2.2.

### 3.3 A 5th-order finite difference scheme in 2D

In Shu and Osher [39], an efficient finite difference ENO scheme is developed for uniform rectangular grid in multi space dimensions. It only uses a 1D finite volume ENO reconstruction of a function from its 1D cell averages. These 1D cell averages are set to

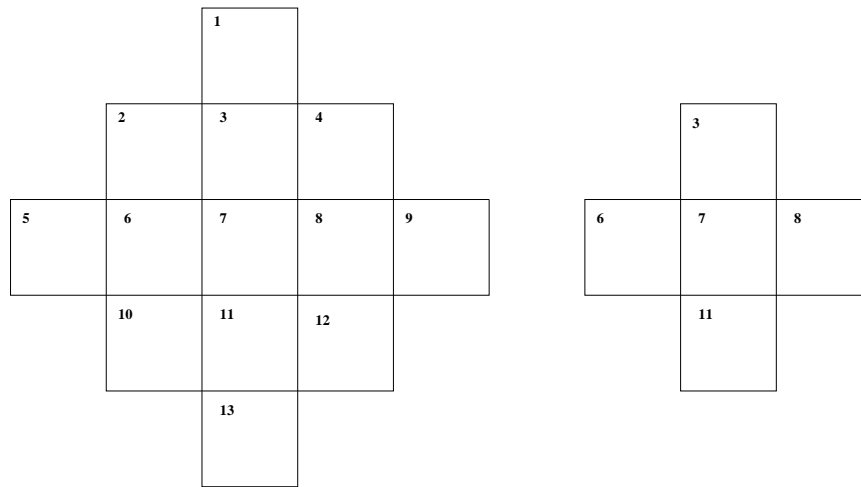


Figure 5: Left: a 4th-order central finite volume reconstruction in cell 7 uses cell averages in cell 1,2,...,13. Right: the hierarchical reconstruction in cell 7 involves only polynomials in cell 3,6,7,8,11.

be equal to the point values of a flux function at the corresponding cell centers. Characteristic decomposition is necessary for higher-order reconstructions, such as the fifth-order ENO or WENO reconstruction, to avoid spurious oscillations. Here we use the finite difference framework of [39] and combine it with the 1D fifth-order central finite volume reconstruction in Section 3.1 followed by the 1D hierarchical reconstruction (see Section 4). This modified finite difference scheme is implemented without characteristic decomposition.

#### 4 Non-oscillatory hierarchical reconstruction

The central reconstruction out of nearby cell averages generates a polynomial in each cell. However, the solution of nonlinear conservation laws may contain discontinuities, and the Gibbs phenomenon could appear in reconstructed polynomials. We are going to apply the non-oscillatory hierarchical reconstruction procedure developed in [29] to remove the possible oscillations and achieve higher resolution near discontinuities. This technique has been developed for the central discontinuous Galerkin formulation in [29]. We show that it also works for finite volume schemes with simple central reconstructions.

From the central or finite volume schemes with the SSP Runge-Kutta time stepping methods, we obtain a piece-wise polynomial solution  $U(\mathbf{x})$  (and  $V(\mathbf{x})$  for dual cells in overlapping grids) at a Runge-Kutta stage, after applying central reconstructions. For example, for the uniform overlapping grid (see Fig. 1 for 2D case), we can write

$$U(\mathbf{x}) = \sum_{I+1/2} U_{I+1/2}(\mathbf{x} - \mathbf{x}_{I+1/2}) \mathbf{1}_{C_{I+1/2}}(\mathbf{x}) \in \mathcal{M} \quad \text{and} \quad V(\mathbf{x}) = \sum_I V_I(\mathbf{x} - \mathbf{x}_I) \mathbf{1}_{D_I}(\mathbf{x}) \in \mathcal{N},$$

recalling that  $\mathbf{x}_{I+1/2}$  and  $\mathbf{x}_I$  are centroids of cell  $C_{I+1/2}$  and  $D_I$  respectively;  $U_{I+1/2}(\mathbf{x} -$

$\mathbf{x}_{I+1/2}$ ) and  $V_I(\mathbf{x}-\mathbf{x}_I)$  are the polynomials (of degree  $r$ ) in cells  $C_{I+1/2}$  and  $D_I$  respectively. The task is to reconstruct a 'limited' version of the polynomial in cell  $C_{I+1/2}$ , retaining high-order accuracy and removing spurious oscillations. For convenience the adjacent cells are renamed as the set  $\{C_J\}$  (which contain cell  $C_{I+1/2}$ ,  $D_I$  etc), and the polynomials (of degree  $r$ ) supported on them are thus renamed as  $\{U_J(\mathbf{x}-\mathbf{x}_J)\}$  respectively, where  $\mathbf{x}_J$  is the cell centroid of cell  $C_J$ . We write  $U_{I+1/2}(\mathbf{x}-\mathbf{x}_{I+1/2})$  in terms of its Taylor expansion,

$$U_{I+1/2}(\mathbf{x}-\mathbf{x}_{I+1/2}) = \sum_{m=0}^r \sum_{|\mathbf{m}|=m} \frac{1}{\mathbf{m}!} U_{I+1/2}^{(\mathbf{m})}(\mathbf{0})(\mathbf{x}-\mathbf{x}_{I+1/2})^{\mathbf{m}},$$

where  $\frac{1}{\mathbf{m}!} U_{I+1/2}^{(\mathbf{m})}(\mathbf{0})$  are the coefficients which participate in its typical  $m$ -degree terms,

$$\sum_{|\mathbf{m}|=m} \frac{1}{\mathbf{m}!} U_{I+1/2}^{(\mathbf{m})}(\mathbf{0})(\mathbf{x}-\mathbf{x}_{I+1/2})^{\mathbf{m}}, \quad |\mathbf{m}|=0, \dots, r.$$

In the following, we briefly describe the hierarchical reconstruction procedure to recompute the polynomial  $U_{I+1/2}(\mathbf{x}-\mathbf{x}_{I+1/2})$  by using polynomials in cells  $\{C_J\}$ . It describes a procedure to compute the new coefficients

$$\frac{1}{\mathbf{m}!} \tilde{U}_{I+1/2}^{(\mathbf{m})}(\mathbf{0}), \quad m=r, r-1, \dots, 0$$

in  $U_{I+1/2}(\mathbf{x}-\mathbf{x}_{I+1/2})$ , iterating from the highest to the lowest degree terms.

To reconstruct  $\tilde{U}_{I+1/2}^{(\mathbf{m})}(\mathbf{0})$ , we first compute many *candidates* of  $U_{I+1/2}^{(\mathbf{m})}(\mathbf{0})$  (sometimes still denoted as  $\tilde{U}_{I+1/2}^{(\mathbf{m})}(\mathbf{0})$  with specification), and we then let the new coefficient for  $U_{I+1/2}^{(\mathbf{m})}(\mathbf{0})$  be

$$\tilde{U}_{I+1/2}^{(\mathbf{m})}(\mathbf{0}) = F(\text{candidates of } U_{I+1/2}^{(\mathbf{m})}(\mathbf{0})),$$

where  $F$  is a convex limiter of its arguments.

In order to find these candidates of  $U_{I+1/2}^{(\mathbf{m})}(\mathbf{0})$ ,  $|\mathbf{m}|=m$ , we take a  $(m-1)$ -th-order partial derivative of  $U_{I+1/2}(\mathbf{x}-\mathbf{x}_{I+1/2})$ , and denote it by

$$\partial^{m-1} U_{I+1/2}(\mathbf{x}-\mathbf{x}_{I+1/2}) = L_{I+1/2}(\mathbf{x}-\mathbf{x}_{I+1/2}) + R_{I+1/2}(\mathbf{x}-\mathbf{x}_{I+1/2}),$$

where  $L_{I+1/2}$  is the linear part and  $R_{I+1/2}$  is the remainder. Clearly, a 'candidate' for a coefficient in the first degree terms of  $L_{I+1/2}$  is the candidate for the corresponding  $U_{I+1/2}^{(\mathbf{m})}(\mathbf{0})$ .

In order to find the candidates for all the coefficients in the first degree terms of  $L_{I+1/2}(\mathbf{x}-\mathbf{x}_{I+1/2})$ , we only need to know the *new approximate cell averages* of  $L_{I+1/2}(\mathbf{x}-\mathbf{x}_{I+1/2})$  on  $d+1$  distinct mesh cells adjacent to cell  $C_{I+1/2}$ , where  $d$  is the spatial dimension. The set of these  $d+1$  cells with given new approximate cell averages is called a *stencil*.

It is shown in [29] the approximation order of accuracy of a polynomial in a cell is unaffected by the algorithm.

Algorithm 4.1:

**Step 1.** Suppose  $r \geq 2$ . For  $m = r, r-1, \dots, 2$ , do the following:

- a. Take a  $(m-1)$ -th-order partial derivative for each of  $\{U_J(\mathbf{x}-\mathbf{x}_J)\}$  to obtain polynomials  $\{\partial^{m-1}U_J(\mathbf{x}-\mathbf{x}_J)\}$  respectively. In particular, denote  $\partial^{m-1}U_{I+1/2}(\mathbf{x}-\mathbf{x}_{I+1/2}) = L_{I+1/2}(\mathbf{x}-\mathbf{x}_{I+1/2}) + R_{I+1/2}(\mathbf{x}-\mathbf{x}_{I+1/2})$ , where  $L_{I+1/2}(\mathbf{x}-\mathbf{x}_{I+1/2})$  is the linear part of  $\partial^{m-1}U_{I+1/2}(\mathbf{x}-\mathbf{x}_{I+1/2})$  and  $R_{I+1/2}(\mathbf{x}-\mathbf{x}_{I+1/2})$  is the remainder.
- b. Calculate the cell averages of  $\{\partial^{m-1}U_J(\mathbf{x}-\mathbf{x}_J)\}$  on cells  $\{C_J\}$  to obtain  $\{\overline{\partial^{m-1}U_J}\}$  respectively.
- c. Let  $\tilde{R}_{I+1/2}(\mathbf{x}-\mathbf{x}_{I+1/2})$  be the  $R_{I+1/2}(\mathbf{x}-\mathbf{x}_{I+1/2})$  with its coefficients replaced by the corresponding new coefficients. Calculate the cell averages of  $\tilde{R}_{I+1/2}(\mathbf{x}-\mathbf{x}_{I+1/2})$  on cells  $\{C_J\}$  to obtain  $\{\overline{\tilde{R}_J}\}$  respectively.
- d. Let  $\overline{L}_J = \overline{\partial^{m-1}U_J} - \overline{\tilde{R}_J}$  for all  $J$ .
- e. Form stencils out of the new approximate cell averages  $\{\overline{L}_J\}$  by using a non-oscillatory finite volume MUSCL or second-order ENO strategy. Each stencil will determine a set of candidates for the coefficients in the first degree terms of  $L_{I+1/2}(\mathbf{x}-\mathbf{x}_{I+1/2})$ , which are also candidates for the corresponding  $U_{I+1/2}^{(\mathbf{m})}(\mathbf{0})$ 's,  $|\mathbf{m}| = m$ .
- f. Repeat from (a) to (e) until all possible combinations of the  $(m-1)$ -th-order partial derivatives are taken. Then the candidates for all coefficients in the  $m$ -th degree terms of  $U_{I+1/2}(\mathbf{x}-\mathbf{x}_{I+1/2})$  have been computed. For each of these coefficients, say  $\frac{1}{\mathbf{m}!}U_{I+1/2}^{(\mathbf{m})}(\mathbf{0})$ ,  $|\mathbf{m}| = m$ , let the new coefficient  $\tilde{U}_{I+1/2}^{(\mathbf{m})}(\mathbf{0}) = F(\text{candidates of } U_{I+1/2}^{(\mathbf{m})}(\mathbf{0}))$ , where  $F$  is a convex limiter.

**Step 2.** In order to find the new coefficients in the zero-th and first-degree terms of  $U_{I+1/2}(\mathbf{x}-\mathbf{x}_{I+1/2})$ , we perform the procedure of Step 1 (a)-(f) with  $m=1$ , and make sure that the new approximate cell average  $\overline{L}_{I+1/2}$  is in each of the stencils, which ensures that the cell average of  $U_{I+1/2}(\mathbf{x}-\mathbf{x}_{I+1/2})$  on cell  $C_{I+1/2}$  is not changed with new coefficients. The new coefficient in the zero-th degree term of  $U_{I+1/2}(\mathbf{x}-\mathbf{x}_{I+1/2})$  is  $\overline{L}_{I+1/2}$ .

### 4.1 An example for 2D overlapping cells

We briefly describe how to implement the hierarchical reconstruction for the piece-wise cubic polynomial reconstructed in Section 2.2.2. Suppose in cell  $C_j$  (see Fig. 3 right), a cubic polynomial is given as

$$\begin{aligned}
 &U_j(x-x_j, y-y_j) \\
 = &U_j(0,0) + \partial_x U_j(0,0)(x-x_j) + \partial_y U_j(0,0)(y-y_j) + \frac{1}{2}\partial_{xx} U_j(0,0)(x-x_j)^2 \\
 &+ \partial_{xy} U_j(0,0)(x-x_j)(y-y_j) + \frac{1}{2}\partial_{yy} U_j(0,0)(y-y_j)^2 + \frac{1}{6}\partial_{xxx} U_j(0,0)(x-x_j)^3 \\
 &+ \frac{1}{2}\partial_{xxy} U_j(0,0)(x-x_j)^2(y-y_j) + \frac{1}{2}\partial_{xyy} U_j(0,0)(x-x_j)(y-y_j)^2 + \frac{1}{6}\partial_{yyy} U_j(0,0)(y-y_j)^3,
 \end{aligned}$$

where  $(x_j, y_j)$  is the cell centroid of cell  $C_j$ ,  $j = 4, 5, 7, 9, 10$ .

According to Step 1 of Algorithm 4.1 with  $m = 3$ , first take the  $(m-1 = 2)$  2nd-order

partial derivative  $\partial_{xx}$  for them to obtain

$$L_j(x-x_j, y-y_j) = \partial_{xx}U_j(0,0) + \partial_{xxx}U_j(0,0)(x-x_j) + \partial_{xxy}U_j(0,0)(y-y_j), \quad j=4,5,7,9,10.$$

Calculate the cell average of  $L_j(x-x_j, y-y_j)$  on cell  $C_j$  to obtain  $\bar{L}_j = \partial_{xx}U_j(0,0)$ ,  $j=4,5,7,9,10$  (note that  $R_7(x-x_7, y-y_7) \equiv 0$ ). With the five new approximate cell averages  $\{\bar{L}_j: j=4,5,7,9,10\}$ , one can apply a MUSCL or a second-order ENO procedure to reconstruct a non-oscillatory linear polynomial

$$\tilde{L}_7(x-x_7, y-y_7) = \partial_{xx}\tilde{U}_7(0,0) + \partial_{xxx}\tilde{U}_7(0,0)(x-x_7) + \partial_{xxy}\tilde{U}_7(0,0)(y-y_7)$$

in cell  $C_7$ . In fact, we form four stencils  $\{C_7, C_4, C_5\}$ ,  $\{C_7, C_5, C_{10}\}$ ,  $\{C_7, C_{10}, C_9\}$  and  $\{C_7, C_9, C_4\}$ . For the first stencil, solve the following equations for  $\partial_{xxx}\tilde{U}_7(0,0)$  and  $\partial_{xxy}\tilde{U}_7(0,0)$ :

$$\frac{1}{|C_j|} \int_{C_j} \tilde{L}_7(x-x_7, y-y_7) dx dy = \bar{L}_7 + \partial_{xxx}\tilde{U}_7(0,0)(x_j-x_7) + \partial_{xxy}\tilde{U}_7(0,0)(y_j-y_7) = \bar{L}_7,$$

$j=4,5$ , similarly for other stencils. We obtain two sets of candidates for  $\partial_{xxx}U_7(0,0)$  and  $\partial_{xxy}U_7(0,0)$  respectively. By taking the 2nd-order partial derivative  $\partial_{xy}$  for  $U_j(x-x_j, y-y_j)$ ,  $j=4,5,7,9,10$ , we similarly obtain a set of candidates for  $\partial_{xyy}U_7(0,0)$  and enlarge the set of candidates for  $\partial_{xxy}U_7(0,0)$ . Taking the 2nd-order partial derivative  $\partial_{yy}$  for  $U_j(x-x_j, y-y_j)$ ,  $j=4,5,7,9,10$ , yields a set of candidates for  $\partial_{yyy}U_7(0,0)$  and enlarge the set of candidates for  $\partial_{xyy}U_7(0,0)$ . Putting all candidates for  $\partial_{xxx}U_7(0,0)$  into the arguments of a limiter function  $F(\cdot)$ , we obtain the new coefficient  $\partial_{xxx}\tilde{U}_7(0,0)$  for  $\partial_{xxx}U_7(0,0)$ . Applying the same procedure to obtain new coefficients  $\partial_{xxy}\tilde{U}_7(0,0)$ ,  $\partial_{xyy}\tilde{U}_7(0,0)$  and  $\partial_{yyy}\tilde{U}_7(0,0)$ .

Repeat the above procedure with  $m=2$ . Note that the  $R_7(x-x_7, y-y_7)$  term as defined in Algorithm 4.1 is non trivial now. For example, taking the 1st derivative  $\partial_x$  for  $U_j(x-x_j, y-y_j)$ ,  $j=4,5,7,9,10$ , we obtain

$$\begin{aligned} & \partial_x U_j(x-x_j, y-y_j) \\ &= \partial_x U_j(0,0) + \partial_{xx}U_j(0,0)(x-x_j) + \partial_{xy}U_j(0,0)(y-y_j) + \frac{1}{2}\partial_{xxx}U_j(0,0)(x-x_j)^2 \\ & \quad + \partial_{xxy}U_j(0,0)(x-x_j)(y-y_j) + \frac{1}{2}\partial_{xyy}U_j(0,0)(y-y_j)^2 \\ &= L_j(x-x_j, y-y_j) + R_j(x-x_j, y-y_j), \quad j=4,5,7,9,10. \end{aligned}$$

We compute the cell average of  $\partial_x U_j(x-x_j, y-y_j)$  on cell  $C_j$  to obtain  $\overline{\partial_x U_j}$ ,  $j=4,5,7,9,10$ ; and compute cell averages of the polynomial

$$\begin{aligned} & \tilde{R}_7(x-x_7, y-y_7) \\ &= \frac{1}{2}\partial_{xxx}\tilde{U}_7(0,0)(x-x_7)^2 + \partial_{xxy}\tilde{U}_7(0,0)(x-x_7)(y-y_7) + \frac{1}{2}\partial_{xyy}\tilde{U}_7(0,0)(y-y_7)^2 \end{aligned}$$

on cell  $C_j$  to obtain  $\bar{R}_j$ ,  $j=4,5,7,9,10$ . Redefine  $\bar{L}_j = \overline{\partial_x U_j} - \bar{R}_j$ ,  $j=4,5,7,9,10$ . The same MUSCL or second-order ENO procedure as described previously can be applied to the

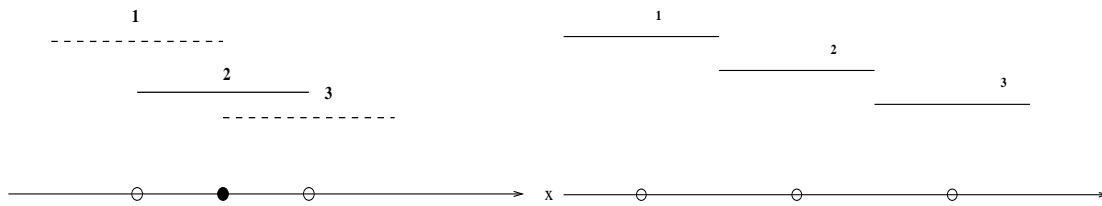


Figure 6: Left: 1D overlapping cells. Right: 1D non-staggered cells. Non-oscillatory hierarchical reconstruction for cell 2 involves only cells 1,2 and 3.

five cell averages  $\{\bar{L}_j; j=4,5,7,9,10\}$  to obtain new coefficients for the first degree terms of  $L_7(x-x_7, y-y_7)$ , namely  $\partial_{xx}\tilde{U}_7(0,0)$  and  $\partial_{xy}\tilde{U}_7(0,0)$ . Then we will take the 1st derivative  $\partial_y$  for  $U_j(x-x_j, y-y_j)$ ,  $j=4,5,7,9,10$ , and so on as described in Algorithm 4.1.

**Remark 4.1.** For the 2D non-staggered mesh, the stencils we use are similar, see Fig. 5 right. One-dimensional hierarchical reconstruction in a cell only involves one adjacent cell on the left and one on the right, regardless the degree of polynomials, see Fig. 6.

### 4.2 Remarks on undershoots

With the hierarchical reconstruction, there could still be some small overshoots or undershoots near discontinuities. For strong shocks, the undershoots could introduce non physical states. We find that in the computation of the double Mach reflection problem ([43], see Section 5), the non staggered finite volume schemes (Section 3) with the hierarchical reconstruction could introduce negative pressure at the shock front, where the pressure ratio across the shock is above 100. We set a lower bound  $p_{low}$  for the pressure, e.g.,  $p_{low} = \frac{3}{4}p_{min}$  where  $p_{min}$  is the estimated lowest pressure ever occurred for the problem. At each time stage of the computation, if the pressure in a cell is below  $p_{low}$ , we redo the hierarchical reconstruction for the cell and its adjacent cells with the new coefficients for the polynomial terms of degrees above one set to be zero in Algorithm 4.1, and recompute the affected cell averages. This reduces the local formal accuracy to second-order in possible trouble regions.

### 4.3 Remarks on limiters

In [29], the convex limiter function  $F()$  used in the hierarchical reconstruction can be the minmod limiter

$$\text{minmod}\{c_1, c_2, \dots, c_m\} = \begin{cases} \min\{c_1, c_2, \dots, c_m\}, & \text{if } c_1, c_2, \dots, c_m > 0, \\ \max\{c_1, c_2, \dots, c_m\}, & \text{if } c_1, c_2, \dots, c_m < 0, \\ 0, & \text{otherwise,} \end{cases} \quad (4.1)$$

so that the linear reconstruction at each stage is a MUSCL reconstruction; or it can be

$$\text{minmod}_2\{c_1, c_2, \dots, c_m\} = c_j, \text{ if } |c_j| = \min\{|c_1|, |c_2|, \dots, |c_m|\} \quad (4.2)$$

so that linear reconstruction at each stage is a second-order ENO reconstruction. In certain situations these limiters used in the hierarchical reconstruction could degenerate the accuracy for approximating smooth solutions. This is due to the abrupt shift of stencils which reduces the smoothness of the numerical flux. Following [34, 37], we can perturb the limiters slightly so that they become center-biased. Define the center-biased minmod limiter to be

$$\text{minmod}_{1,1}\{c_1, c_2, \dots, c_m\} = \text{minmod} \left\{ (1 + \epsilon) \text{minmod}\{c_1, c_2, \dots, c_m\}, \frac{1}{m} \sum_{i=1}^m c_i \right\}, \quad (4.3)$$

where  $\epsilon$  is a small positive number. It is easy to see that  $\text{minmod}_{1,1}$  still returns a convex combination of its arguments, and if  $\epsilon=0$ , it becomes the minmod limiter. For all numerical experiments conducted in the paper, we take  $\epsilon=0.01$  and find that it does not increase the overshoots or undershoots at discontinuities significantly, and it slightly improves the resolution of the smooth solution near discontinuities.

#### 4.4 Remarks on the complexity

In the 2D code we have developed for the 4th-order central scheme on overlapping cells (Section 2.2.2) with the hierarchical reconstruction, we find that the hierarchical reconstruction takes about half of the total CPU time. Therefore, using a smoothness detector to turn off the hierarchical reconstruction in smooth regions will effectively reduce the overall complexity. Here we use the low cost smoothness detector in [7]. After the high-degree (of degree  $r$ ) polynomial solution is obtained in each cell by a central reconstruction, the jump of the solution at the center of each cell edge is measured for non-staggered meshes. If the jumps at the edges of a cell are smaller than  $\Delta x^{(r+1)/2}$ , the cell is considered to be in the smooth region and the hierarchical reconstruction will not be performed in the cell; otherwise hierarchical reconstruction will be performed in the cell. For staggered meshes, we only measure the jump at the cluster point of a cell where adjacent overlapping cells join. This smoothness detector is used for all 2D computations (except for accuracy tests for smooth solutions).

## 5 Numerical examples

In the numerical experiments, the third-order SSP Runge-Kutta time discretization method [39] (also frequently called the third-order TVD Runge-Kutta method) is applied to all schemes. When overlapping cells are used, only the solution in one class of the overlapping cells is shown in the graphs throughout this section. For systems of equations, the component-wise extensions of the scalar schemes (without characteristic decomposition) are used in all computations.

Table 1: 5th-order finite volume scheme (Sections 3.1, 4 and (4.1)) for the 1D Burgers' equation.

$\Delta x$	1/10	1/20	1/40	1/80	1/160
$l_1$ error	0.000138	4.42e-06	1.66e-07	6.77e-09	3.09e-10
order	-	4.96	4.73	4.62	4.45
$l_\infty$ error	0.000201	8.95e-06	4.11e-07	2.33e-08	1.92e-09
order	-	4.49	4.44	4.14	3.60

Table 2: 5th-order central scheme (Sections 2.2.1, 4 and (4.2)) for the 1D Burgers' equation.

$\Delta x$	1/10	1/20	1/40	1/80	1/160
$l_1$ error	1.24e-05	3.81e-07	1.21e-08	3.76e-10	1.18e-11
order	-	5.04	4.98	5.01	4.99
$l_\infty$ error	2.16e-05	7.21e-07	3.28e-08	1.29e-09	5.62e-11
order	-	4.90	4.46	4.67	4.52

**Example 5.1.** The Burgers' equation with periodic boundary conditions:

$$u_t + \left(\frac{1}{2}u^2\right)_x = 0, \quad u(x,0) = \frac{1}{4} + \frac{1}{2}\sin(\pi x).$$

The errors are shown at the final time  $T = 0.1$  when the solution is still smooth. The errors computed by the 5th-order central scheme with hierarchical reconstruction (Sections 2.2.1, 4 and (4.2)) are listed in Table 2, with

$$\Delta\tau^n = \Delta x/1.5, \quad \theta = 1/2, \quad \Delta t^n = \min\{\theta * \Delta\tau^n, \Delta x^{5/3}\}.$$

The errors computed by the 5th-order finite volume scheme with hierarchical reconstruction (Sections 3.1, 4 and (4.1)) are listed in Table 1, with  $\Delta t^n = \min\{CFL * \Delta x/0.75, \Delta x^{5/3}\}$ ,  $CFL = 0.9$ . We can see that these schemes essentially achieve their expected accuracy, at least in the  $l_1$  norm.

**Example 5.2.** The 2D Burgers' equation with periodic boundary conditions:

$$u_t + \left(\frac{1}{2}u^2\right)_x + \left(\frac{1}{2}u^2\right)_y = 0, \quad u(x,0) = \frac{1}{4} + \frac{1}{2}\sin(\pi(x+y)).$$

The errors are shown at the final time  $T = 0.1$  when the solution is still smooth. The errors computed by the 3rd-order central scheme (Sections 2.2.3, 4 and (4.2)) are listed in Table 3, with  $\Delta\tau^n$  determined with CFL number 0.4,  $\theta = 0.9$ . The errors computed by the 4th-order central scheme without hierarchical reconstruction (Section 2.2.2) are listed in Table 4, with  $\Delta\tau^n$  determined with CFL number 0.4,  $\Delta t^n = \min\{0.9 * \Delta\tau^n, \Delta x^{4/3}\}$ . The errors with hierarchical reconstruction (Sections 2.2.2, 4 and (4.2)) are listed in Table 5.

Table 3: 3rd-order central scheme (Sections 2.2.3, 4 and (4.2)) for the 2D Burgers' equation.

$\Delta x$	1/4	1/8	1/16	1/32	1/64
$l_1$ error	8.21E-2	1.27E-2	1.60E-3	1.97E-4	2.43E-5
order	-	2.69	2.99	3.02	3.02
$l_\infty$ error	5.10E-2	9.27E-3	1.62E-3	2.02E-4	2.86E-5
order	-	2.46	2.52	3.00	2.82

Table 4: 4th-order central scheme (Section 2.2.2) for the 2D Burgers' equation.

$\Delta x$	1/4	1/8	1/16	1/32	1/64
$l_1$ error	2.83E-2	2.72E-3	1.85E-4	1.16E-5	7.12E-7
order	-	3.38	3.88	4.00	4.03
$l_\infty$ error	2.27E-2	2.32E-3	2.12E-4	1.43E-5	8.57E-7
order	-	3.29	3.45	3.89	4.06

Table 5: 4th-order central scheme (Sections 2.2.2, 4 and (4.2)) for the 2D Burgers' equation.

$\Delta x$	1/4	1/8	1/16	1/32	1/64
$l_1$ error	6.02E-2	5.91E-3	3.83E-4	2.19E-5	1.44E-6
order	-	3.35	3.95	4.13	3.93
$l_\infty$ error	3.85E-2	4.24E-3	3.24E-4	2.38E-5	1.67E-6
order	-	3.18	3.71	3.77	3.83

The errors computed by the 4th-order finite volume scheme (Sections 3.2, 4 and (4.3)) are listed in Table 6, with  $\Delta t^n$  determined by CFL factor 0.5 or equal to  $\Delta x^{4/3}$ , whichever is smaller. The errors computed by the 5th-order finite difference scheme (Sections 3.3, 4 and (4.3)) are listed in Table 7, with  $\Delta t^n$  determined by CFL factor 0.4 or equal to  $\Delta x^{5/3}$ , whichever is smaller. We can see the errors meet the expectation. In particular, the errors become more consistent when the center biased minmod limiter (4.3) is used.

**Example 5.3.** The 2D Euler equation can written as

$$\mathbf{u}_t + \mathbf{f}(\mathbf{u})_x + \mathbf{g}(\mathbf{u})_y = 0, \quad \mathbf{u} = (\rho, \rho u, \rho v, E)^T, \quad p = (\gamma - 1)(E - \frac{1}{2}\rho(u^2 + v^2)),$$

$$\mathbf{f}(\mathbf{u}) = (\rho u, \rho u^2 + p, \rho u v, u(E + p))^T, \quad \mathbf{g}(\mathbf{u}) = (\rho v, \rho u v, \rho v^2 + p, v(E + p))^T,$$

where  $\gamma = 1.4$ . There is a set of exact solution (and thus the initial value) given by  $\rho = 1 + 0.5 \sin(x + y - (u + v)t)$ ,  $u = 1$ ,  $v = -0.7$  and  $p = 1$ .

We conduct a convergence test for the 4th-order central scheme (Sections 2.2.2, 4 and (4.3)) on an irregular mesh on the spatial domain  $[0, 1] \times [0, 1]$ , from the time  $T = 0$  to  $T = 0.1$ . The irregular staggered mesh is such that for one class of the overlapping cells, the cell size is  $\Delta x = \Delta y = h$  in the upper half domain and is  $\Delta x = 2\Delta y = h$  in the lower half domain.

Table 6: 4th-order finite volume scheme (Sections 3.2, 4 and (4.3)) for the 2D Burgers' equation.

$\Delta x$	1/4	1/8	1/16	1/32	1/64
$l_1$ error	6.34E-2	5.93E-3	3.07E-4	1.35E-5	7.35E-7
order	-	3.42	4.27	4.51	4.20
$l_\infty$ error	4.25E-2	4.66E-3	2.54E-4	1.63E-5	1.27E-6
order	-	3.19	4.20	3.96	3.68

Table 7: 5th-order finite difference scheme (Sections 3.3, 4 and (4.3)) for the 2D Burgers' equation.

$\Delta x$	1/4	1/8	1/16	1/32	1/64
$l_1$ error	7.42E-2	4.22E-3	5.95E-05	2.40E-6	4.26E-8
order	-	4.13	6.15	4.63	5.82
$l_\infty$ error	4.14E-2	4.63E-3	1.17E-4	5.45E-6	1.68E-7
order	-	3.16	5.31	4.42	5.02

Table 8: 4th-order central scheme (Sections 2.2.2, 4 and (4.3)) on an irregular overlapping mesh (such that for one class of cells,  $\Delta x = \Delta y = h$  in the upper half domain and  $\Delta x = 2\Delta y = h$  in the lower half domain) for the 2D Euler equation.

$h$	1/4	1/8	1/16	1/32	1/64
$l_1$ error	5.84E-5	3.77E-6	2.36E-7	1.55E-8	1.26E-9
order	-	3.95	4.00	3.93	3.62
$l_\infty$ error	2.15E-4	2.50E-5	2.63E-6	3.12E-7	3.54E-8
order	-	3.10	3.25	3.08	3.14

The density errors are shown at the final time in Table 8. We can see that in the  $l_1$  norm, the errors meet the expectation for the irregular mesh.

**Example 5.4.** We compute the 1D Euler equation with Lax's initial data.  $u_t + f(u)_x = 0$  with  $u = (\rho, \rho v, E)^T$ ,  $f(u) = (\rho v, \rho v^2 + p, v(E + p))^T$ ,  $p = (\gamma - 1)(E - \frac{1}{2}\rho v^2)$ ,  $\gamma = 1.4$ . Initially, the density  $\rho$ , momentum  $\rho v$  and total energy  $E$  are 0.445, 0.311 and 8.928 in  $(0, 0.5)$ ; 0.5, 0 and 1.4275 in  $(0.5, 1)$ .

The computed density profiles by various numerical schemes with hierarchical reconstruction are shown at  $T = 0.16$  in Fig. 7 with  $\Delta x = 1/200$ . For central schemes on overlapping cells,  $\Delta \tau^n$  is chosen with CFL factor 0.4,  $\Delta t^n = 0.5\Delta \tau^n$ . For finite volume schemes,  $\Delta t^n$  is determined with CFL factor 0.9. The solid line is the numerical solution on a fine mesh ( $\Delta x = 1/1000$ ) computed by a central scheme on overlapping cells [28]. Compared with the 5th-order WENO scheme without characteristic decomposition, the hierarchical reconstruction has essentially no spurious oscillations but small overshoots. However, the 5th-order WENO scheme with characteristic decomposition gives the best result.

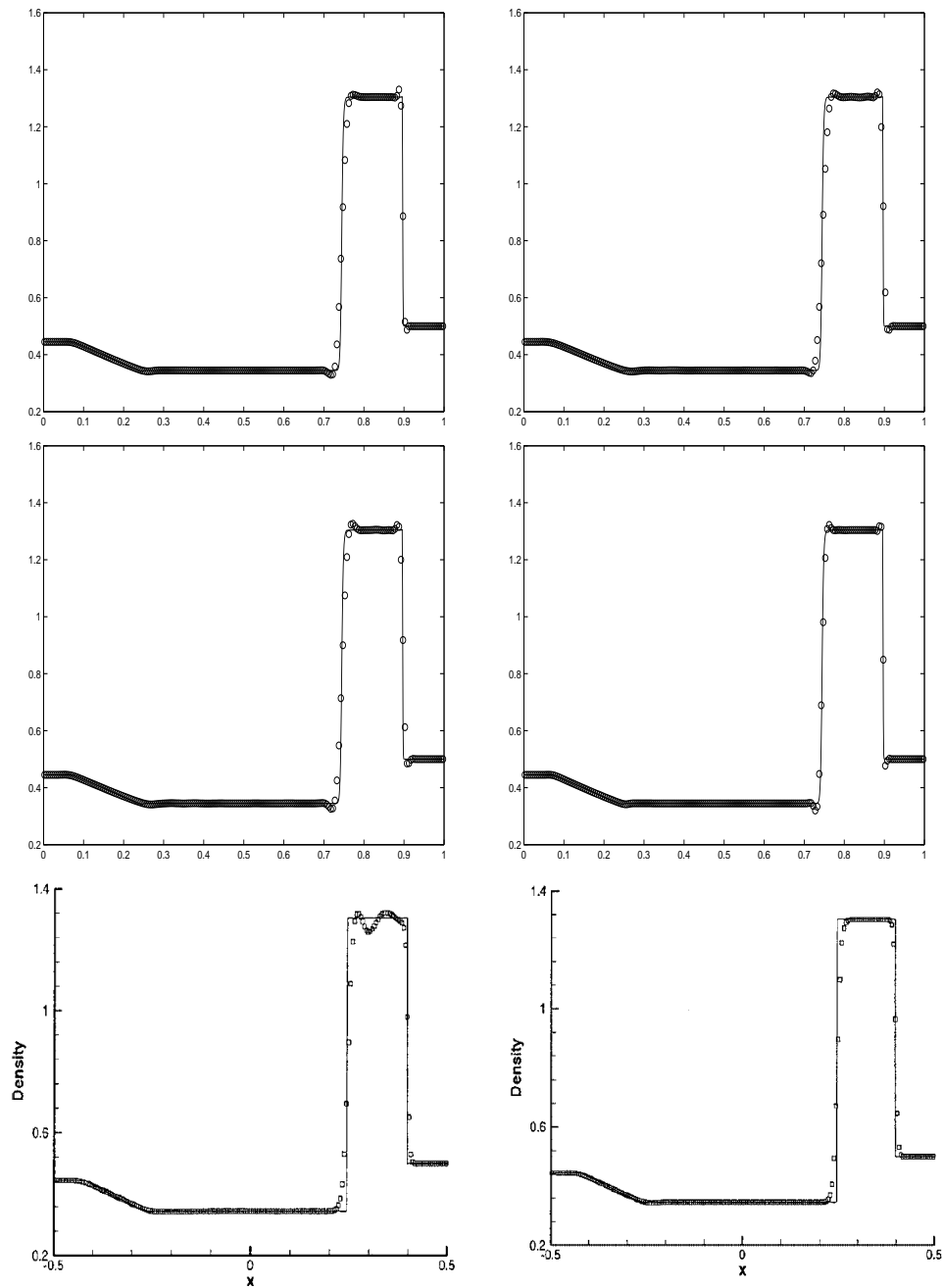


Figure 7: Comparative results of density for Lax's Problem,  $\Delta x=1/200$ . From left to right, top to bottom. (1) 3rd-order central scheme (Sections 2.2.3, 4 and (4.2)); (2) 5th-order finite volume scheme (Sections 3.1, 4 and (4.1)); (3) 5th-order finite volume scheme (Sections 3.1, 4 and (4.3)); (4) 5th-order central scheme (Sections 2.2.1, 4 and (4.2)); (5) 5th-order WENO scheme (reprinted from [31], Copyright (2002), with permission from Elsevier); (6) 5th-order WENO scheme with characteristic decomposition (reprinted from [31], Copyright (2002), with permission from Elsevier).

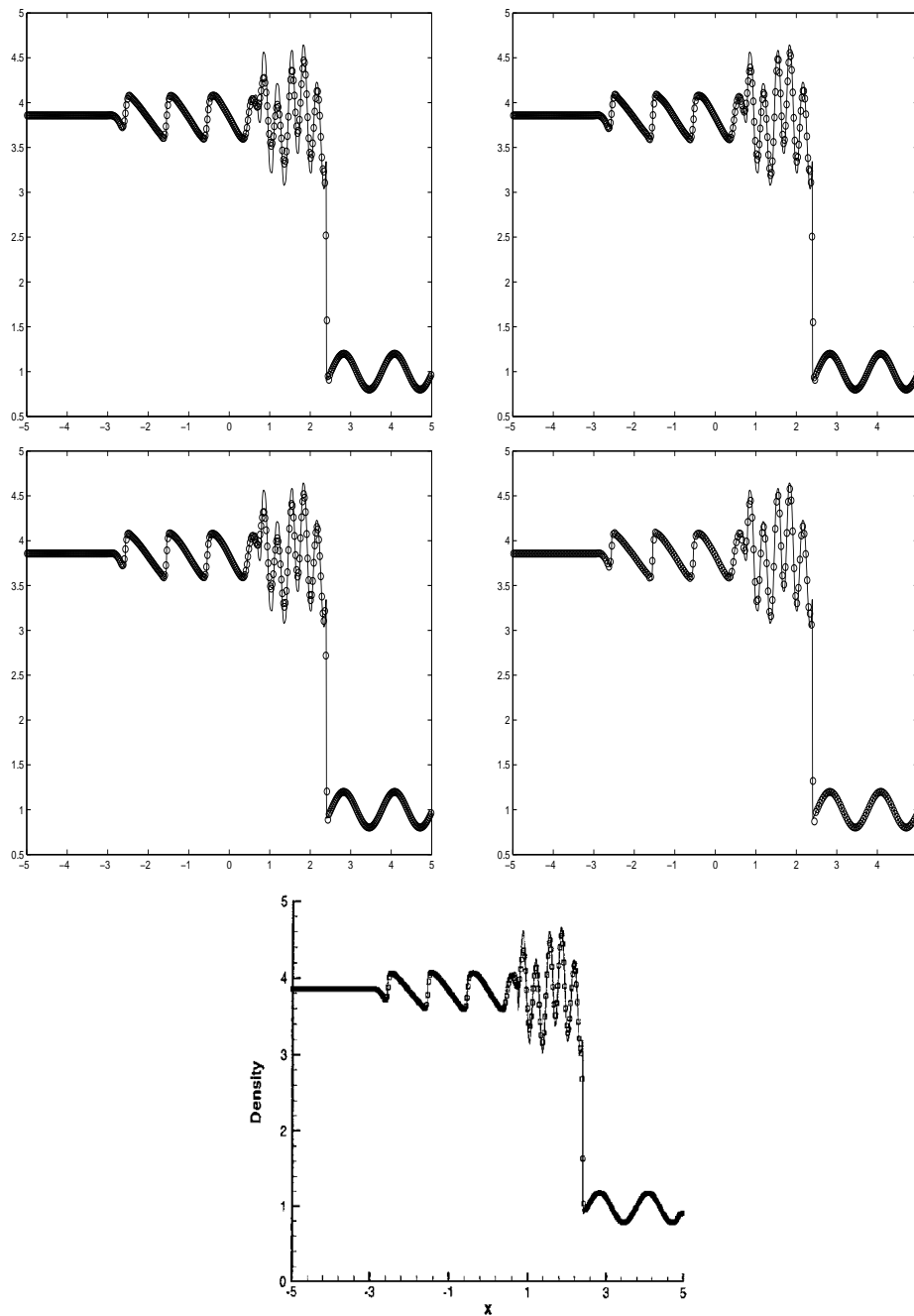


Figure 8: Shu-Osher Problem,  $\Delta x = 1/40$  by default. From left to right, top to bottom, (1) 5th-order finite volume scheme (Sections 3.1, 4 and (4.1)); (2) 5th-order finite volume scheme (Sections 3.1, 4 and (4.3)); (3) 3rd-order central scheme (Sections 2.2.3, 4 and (4.2)); (4) 5th-order central scheme (Sections 2.2.1, 4 and (4.1)),  $\Delta x = 1/28$ ; (5) 5th-order WENO scheme with characteristic decomposition (reprinted from [31], Copyright (2002), with permission from Elsevier).

**Example 5.5.** Shu-Osher problem [40]. It is the Euler equation with initial data

$$\begin{aligned}(\rho, v, p) &= (3.857143, 2.629369, 10.333333), \quad \text{for } x < -4, \\(\rho, v, p) &= (1 + 0.2\sin(5x), 0, 1), \quad \text{for } x \geq -4.\end{aligned}$$

The density profiles computed by various numerical schemes with hierarchical reconstruction are plotted at  $T = 1.8$ , with  $\Delta x = 1/40$  by default, see Fig. 8. For central schemes on overlapping cells,  $\Delta\tau^n$  is chosen with CFL factor 0.5,  $\Delta t^n = 0.5\Delta\tau^n$ . For finite volume schemes,  $\Delta t^n$  is determined with CFL factor 0.9. The solid line is the numerical solution on a fine mesh ( $\Delta x = 1/200$ ) computed by a central scheme on overlapping cells [28]. We can see that the resolution of 5th-order finite volume schemes with hierarchical reconstruction gets close to that of the 5th-order WENO scheme. The central schemes on overlapping cells with hierarchical reconstruction produce better resolution because twice as many cells are used.

**Example 5.6.** Woodward and Colella problem [43] for the Euler equation computed by various numerical schemes with hierarchical reconstruction. Initially, the density, momentum, total energy are 1,0,2500 in  $(0,0.1)$ ; 1,0,0.025 in  $(0.1,0.9)$ ; 1,0,250 in  $(0.9,1)$ .

For central schemes on overlapping cells,  $\Delta\tau^n$  is chosen with CFL factor 0.4,  $\Delta t^n = 0.5\Delta\tau^n$ . For finite volume schemes,  $\Delta t^n$  is determined with CFL factor 0.5. Comparison of density profiles at  $T = 0.01$  and  $T = 0.038$  of different schemes with hierarchical reconstruction can be found in Fig. 9. The solid lines are the numerical solutions on a fine mesh ( $\Delta x = 1/2000$ ) computed by a central scheme on overlapping cells [28]. We can see that by using hierarchical reconstruction, 5th-order schemes without characteristic decomposition can still generate quite stable results for this demanding problem.

**Example 5.7.** Double Mach reflection [43] computed by various numerical schemes with hierarchical reconstruction. A planar Mach 10 shock is incident on an oblique wedge at a  $\pi/3$  angle. The air in front of the shock has density 1.4, pressure 1 and velocity 0. It is described by the 2D Euler equation with  $\gamma = 1.4$ , and the boundary condition is described in [43].

The density profiles are plotted at  $T = 0.2$  in Figs. 10 and 11, with 30 equally spaced contours. For central schemes on overlapping cells,  $\Delta\tau^n$  is chosen with CFL factor 0.45; for finite volume schemes,  $\Delta t^n$  is determined with CFL factor 0.5; for the 5th-order finite difference scheme (Sections 3.3, 4 and (4.3)),  $\Delta t^n$  is determined with CFL factor 0.4. The density along the line  $y = 1/3$  is plotted against  $x$  in Fig. 12, on a mesh with  $\Delta x = \Delta y = 1/120$ . We can see that computed results are non-oscillatory on this mesh.

In Fig. 13, we show the density contour computed by the 5th-order finite difference (Sections 3.3, 4 and (4.3)) on a mesh with  $\Delta x = \Delta y = 1/960$ . In Fig. 14, the 4th-order central scheme (Sections 2.2.2, 4 and (4.2)) is applied to an irregular mesh such that for one class of cells,  $\Delta x = \Delta y = h$  in the upper half domain and  $\Delta x = 2\Delta y = h$  in the lower half domain. We can see in the graph that across the border line  $y = 0.5$  separating two different grids, the horizontal shock becomes thicker while the vertical shock is almost unchanged.

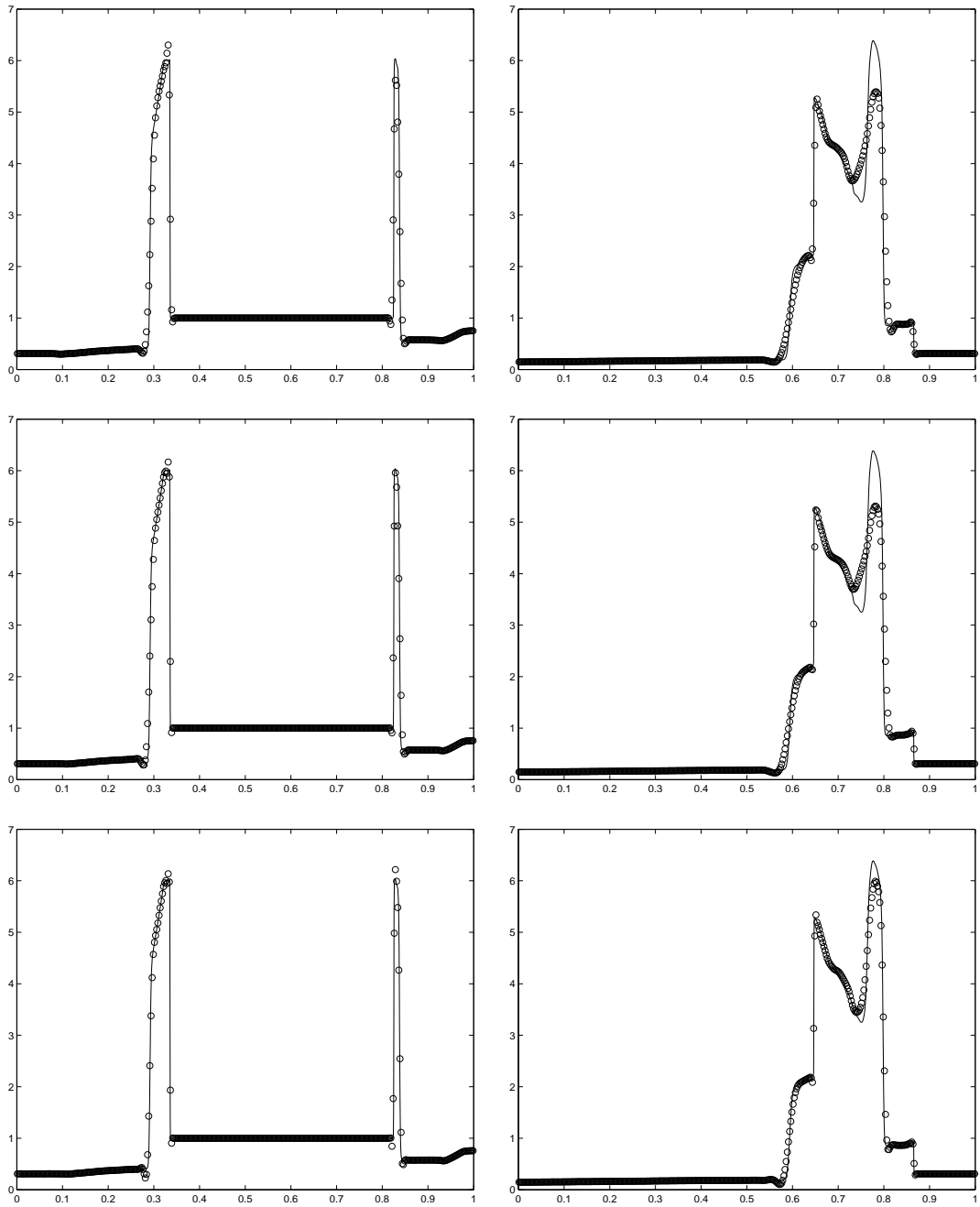


Figure 9: Woodward and Colella Problem. Comparison of density profiles at  $T=0.01$  (left) and  $T=0.038$  (right).  $\Delta x=1/400$ . The 1st row: 5th-order finite volume scheme (Sections 3.1, 4 and (4.3)); 2nd row: 3rd-order central scheme (Sections 2.2.3, 4 and (4.2)); 3rd row: 5th-order central scheme (Sections 2.2.1, 4 and (4.2)).

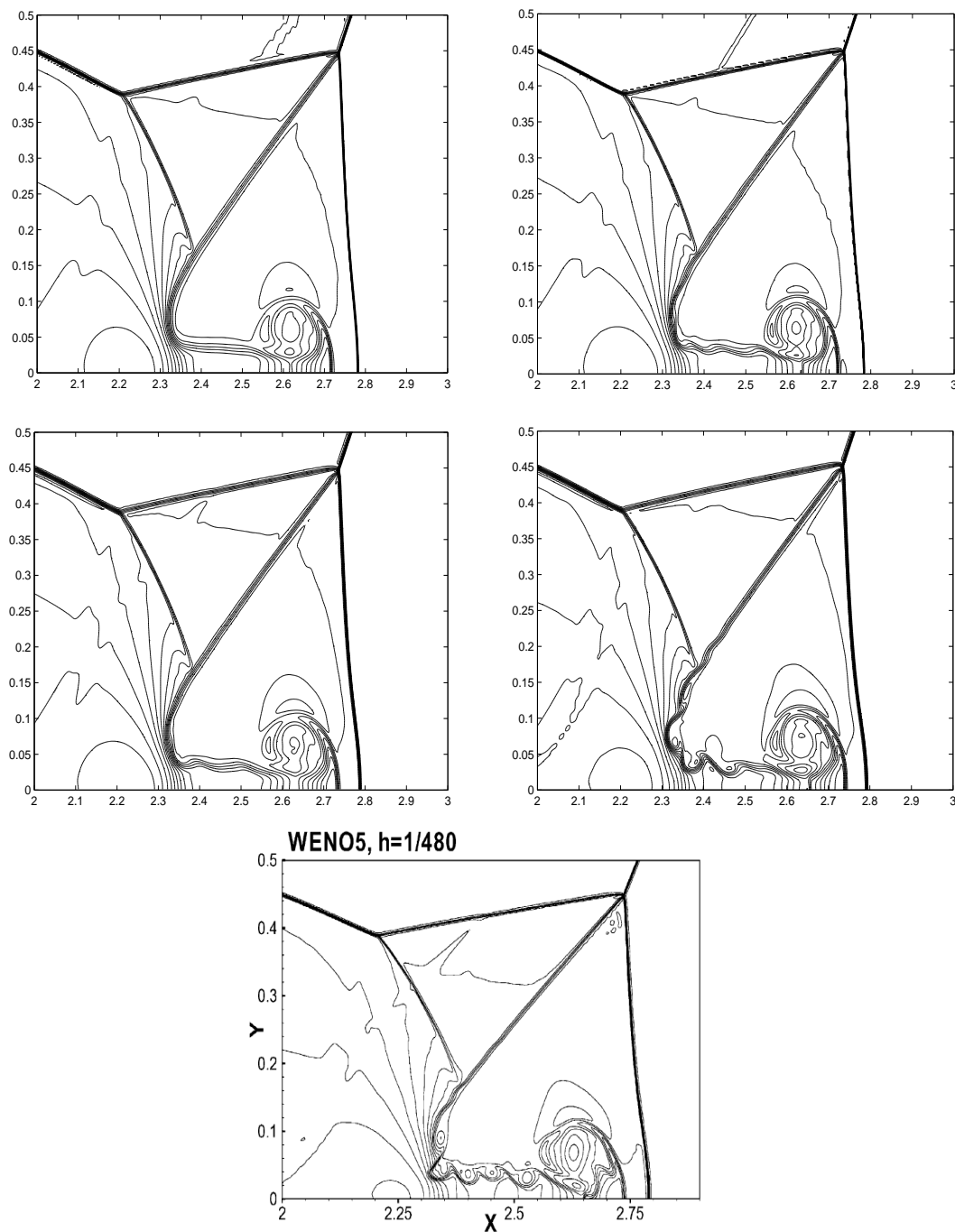


Figure 10: Density contours of the double Mach reflection,  $\Delta x = \Delta y = 1/480$ . From top to bottom, left to right: (1) 3rd-order central scheme (Sections 2.2.3, 4 and (4.2)); (2) 4th-order central scheme (Sections 2.2.2, 4 and (4.2)); (3) 4th-order finite volume scheme (Sections 3.2, 4 and (4.3)); (4) 5th-order finite difference scheme (Sections 3.3, 4 and (4.3)); (5) 5th-order WENO scheme with characteristic decomposition (reprinted from [36], Copyright (2003), with permission from Elsevier).

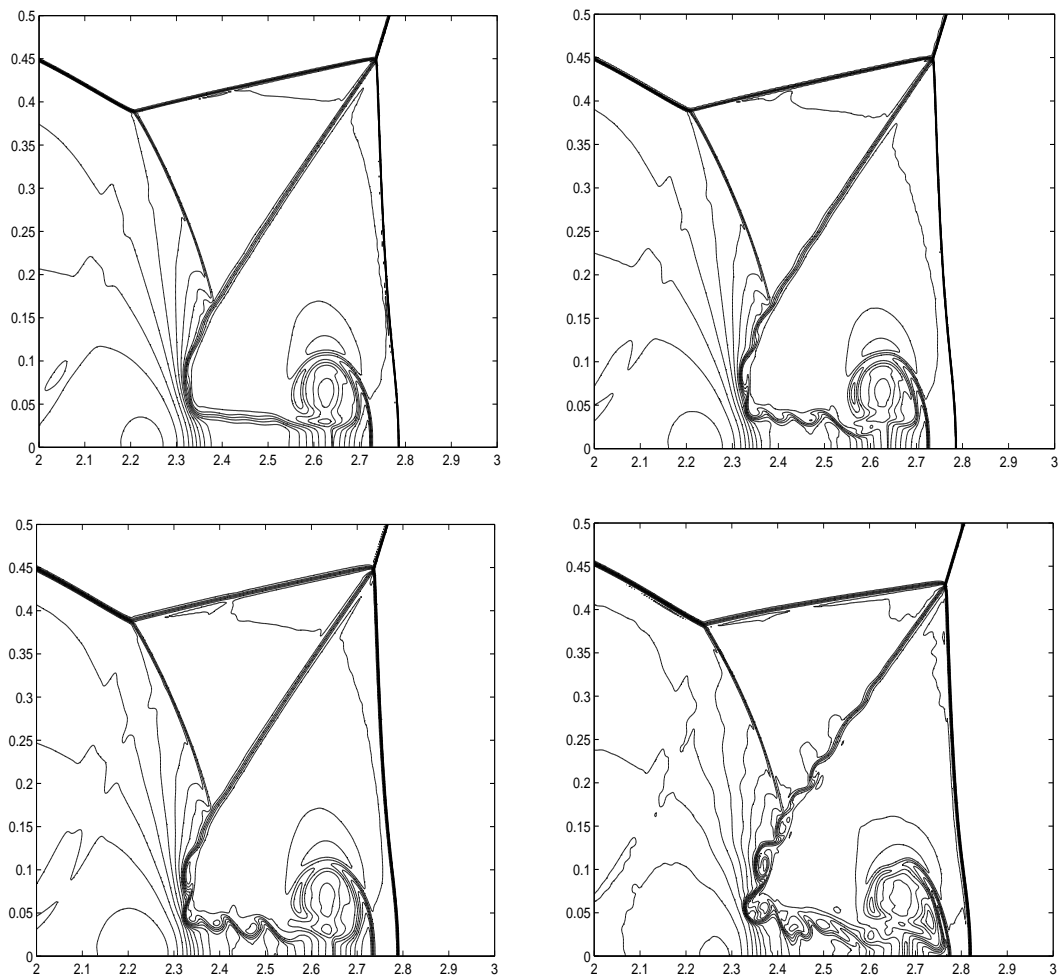


Figure 11: Density contours of the double Mach reflection,  $\Delta x = \Delta y = 1/600$  by default. From top to bottom, left to right: (1) 3rd-order central scheme (Sections 2.2.3, 4 and (4.2)),  $\Delta x = \Delta y = 1/720$ ; (2) 4th-order central scheme (Sections 2.2.2, 4 and (4.2)); (3) 4th-order finite volume scheme (Sections 3.2, 4 and (4.3)); (4) 5th-order finite difference scheme (Sections 3.3, 4 and (4.3)).

We can see that the 5th-order scheme with hierarchical reconstruction produces similar results near the contact line as the 5th-order WENO scheme with characteristic decomposition does.

**Example 5.8.** 2D Riemann problem [24] for the Euler equation. The computational domain is  $[0,1] \times [0,1]$ . The initial states are constants within each of the 4 quadrants. Counter-clock-wisely from the upper right quadrant, they are labeled as  $(\rho_i, u_i, v_i, p_i)$ ,  $i = 1, 2, 3, 4$ . Initially,  $\rho_1 = 1.1$ ,  $u_1 = 0$ ,  $v_1 = 0$ ,  $p_1 = 1.1$ ;  $\rho_2 = 0.5065$ ,  $u_2 = 0.8939$ ,  $v_2 = 0$ ,  $p_2 = 0.35$ ;  $\rho_3 = 1.1$ ,  $u_3 = 0.8939$ ,  $v_3 = 0.8939$ ,  $p_3 = 1.1$ ;  $\rho_4 = 0.5065$ ,  $u_4 = 0$ ,  $v_4 = 0.8939$ ,  $p_4 = 0.35$ .

We want to further check two schemes for the problem: the 4th-order central scheme

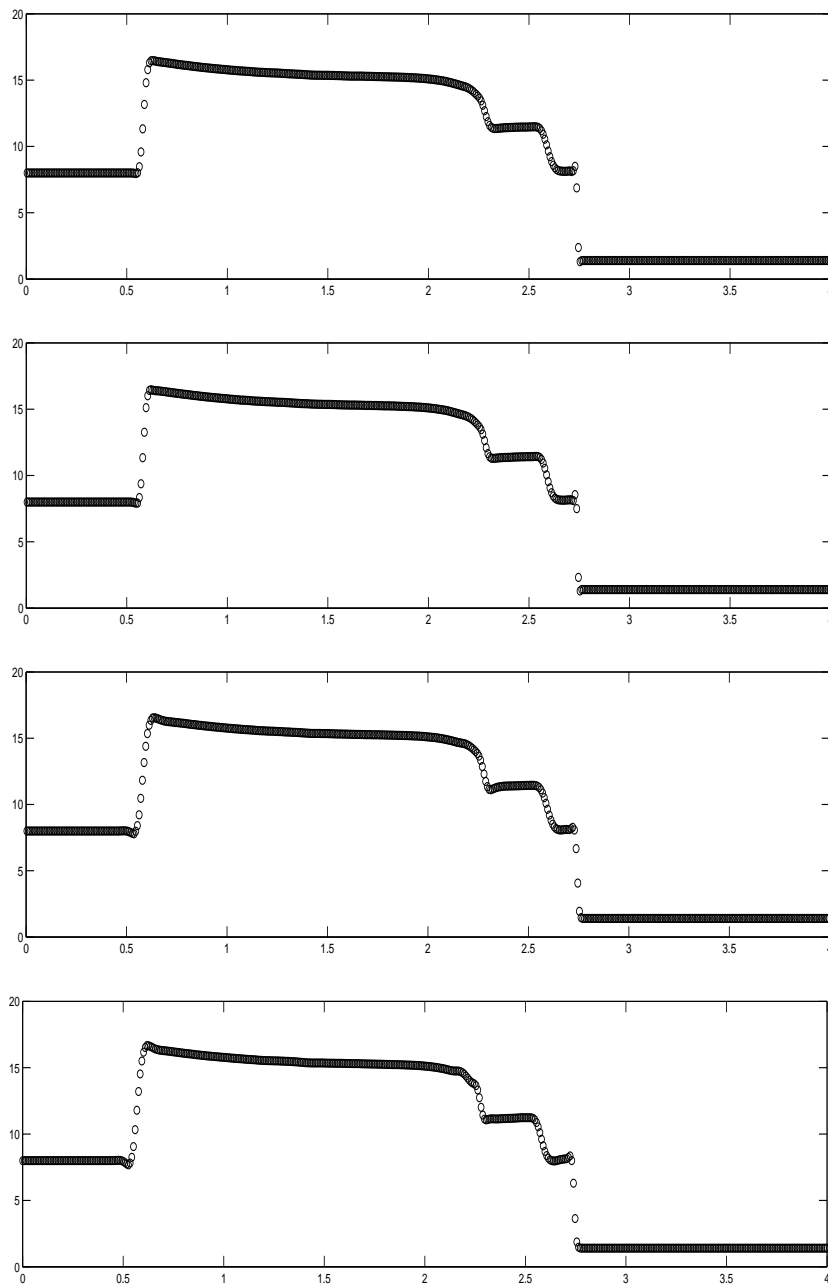


Figure 12: Double Mach reflection on a mesh with  $\Delta x = \Delta y = 1/120$ . Density plot along  $y = 1/3$ . From top to bottom: (1) 3rd-order central scheme (Sections 2.2.3, 4 and (4.2)); (2) 4th-order central scheme (Sections 2.2.2, 4 and (4.2)); (3) 4th-order finite volume scheme (Sections 3.2, 4 and (4.3)); (4) 5th-order finite difference scheme (Sections 3.3, 4 and (4.3)).

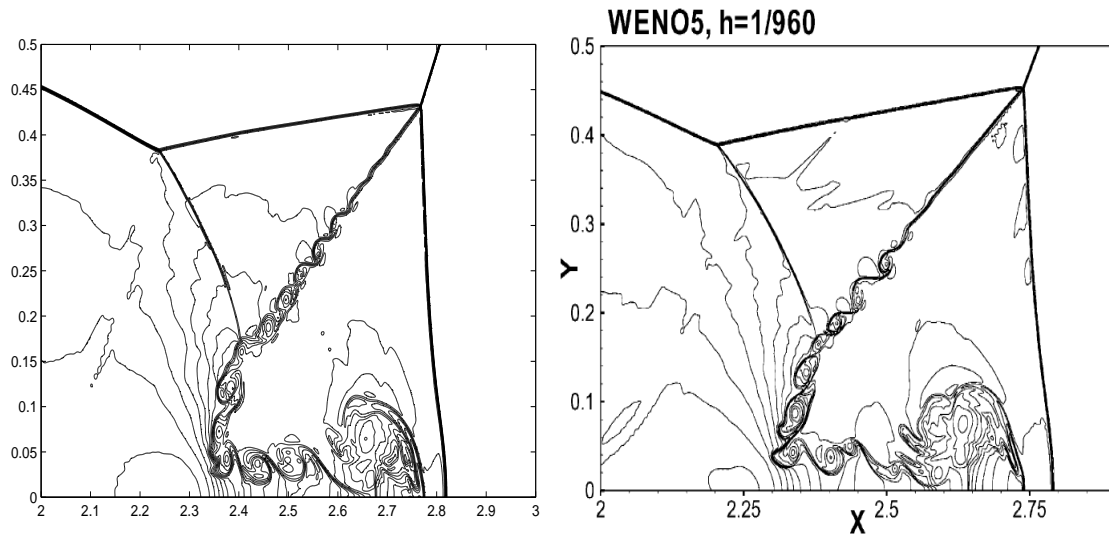


Figure 13: Density contour of the double Mach reflection on a mesh  $\Delta x = \Delta y = 1/960$ . Left: 5th-order finite difference scheme (Sections 3.3, 4 and (4.3)); Right: 5th-order WENO scheme with characteristic decomposition (reprinted from [36], Copyright (2003), with permission from Elsevier).

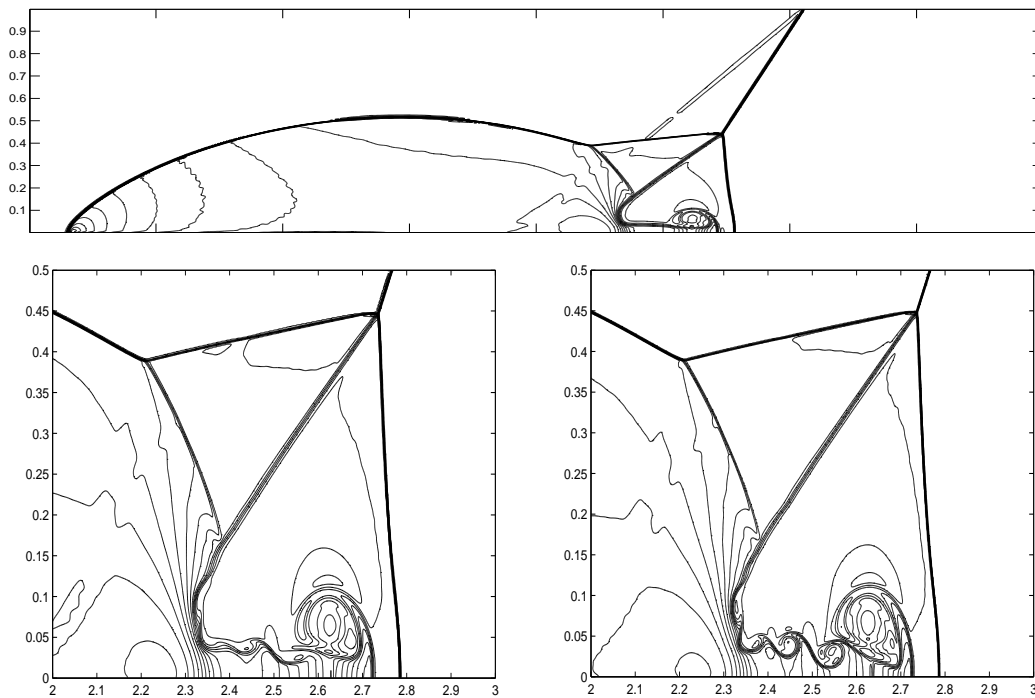


Figure 14: Density contour of the double Mach reflection. Computed on an irregular mesh (such that for one class of cells,  $\Delta x = \Delta y = h$  in the upper half domain and  $\Delta x = 2\Delta y = h$  in the lower half domain) by the 4th-order central scheme (Sections 2.2.2, 4 and (4.3)). Top:  $h = 1/240$ . Bottom left:  $h = 1/400$ . Bottom right:  $h = 1/480$ .

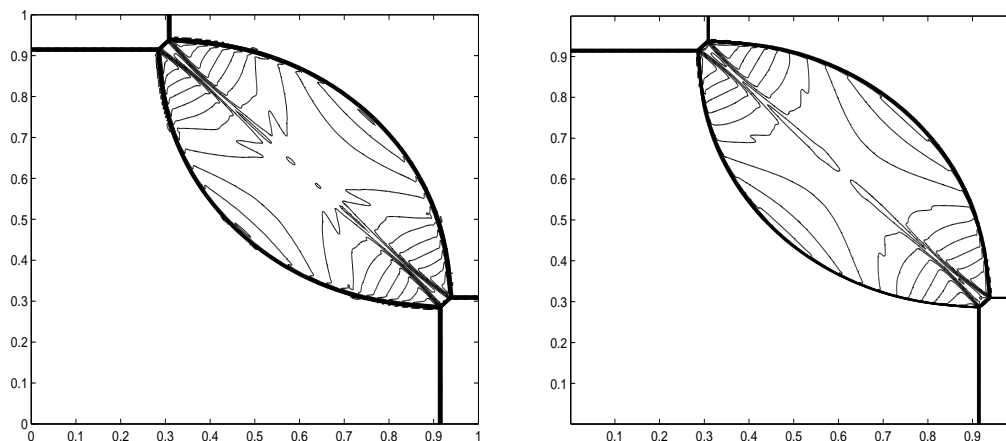


Figure 15: Density contour of a 2D Riemann problem [24]. Left: 5th-order finite difference scheme (Sections 3.3, 4 and (4.3)),  $\Delta x = \Delta y = 1/400$ . Right: 4th-order central scheme (Sections 2.2.2, 4 and (4.3)) on an irregular overlapping mesh such that for one class of the cells,  $\Delta x = \Delta y = 1/400$  in the upper half domain and  $\Delta x = 2\Delta y = 1/400$  in the lower half domain

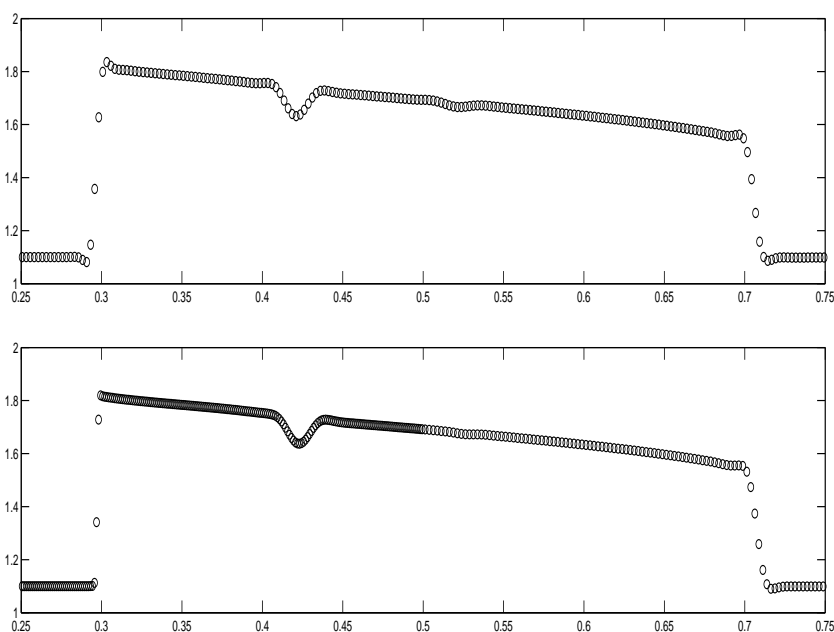


Figure 16: 2D Riemann problem [24]. Density along the line  $x = 0.8$ . Top: 5th-order finite difference scheme (Sections 3.3, 4 and (4.3)). Bottom: 4th-order central scheme (Sections 2.2.2, 4 and (4.3)) on the irregular overlapping mesh.

on irregular overlapping cells and the 5th-order finite difference scheme, both with hierarchical reconstruction. The density contours are plotted at  $T = 0.25$  in Fig. 15, with 40 equally spaced contours. The density profiles along  $x = 0.8$  are plotted in Fig. 16. We can

see that the solutions of these high-order schemes are not oscillatory from these graphs. It should be noticed that lower-order schemes can perform just as well for this problem, see e.g. [23,24].

## 5.1 Remarks on numerical experiments

The CPU time on a 1.8 GHz processor (AMD Opteron 244) for the computation of the double Mach reflection (Example 5.7) on a mesh with  $\Delta x = \Delta y = 1/120$  is 18 minutes for the 5th-order finite difference scheme (Sections 3.3, 4 and (4.3)); 47 minutes for the 4th-order finite volume scheme (Sections 3.2, 4 and (4.3)); 38 minutes for the 3rd-order central scheme on overlapping cells (Sections 2.2.3, 4 and (4.2)); 77 minutes for the 4th-order central scheme on overlapping cells (Sections 2.2.2, 4 and (4.2)). The codes are written in C++ and are compiled by "g++ -O4". The complexity data is highly subjective to the programming and compiler.

Even though central schemes on overlapping cells are more expensive, from our experience they tend to be more robust without characteristic decomposition for higher order: having smaller overshoots/undershoots at discontinuities and smoother solutions elsewhere (e.g., by comparing the constant solutions in  $[0.7,0.9]$  for the Lax problem, Fig. 7). For the non-staggered 4th- and 5th-order schemes we need to fix the negative pressure problem (due to the undershoots) for very strong shocks (Example 5.7).

## Acknowledgments

The research of Y. Liu was supported in part by NSF grant DMS-0511815. The research of C.-W. Shu was supported in part by the Chinese Academy of Sciences while this author was visiting the University of Science and Technology of China (grant 2004-1-8) and the Institute of Computational Mathematics and Scientific/Engineering Computing. Additional support was provided by ARO grant W911NF-04-1-0291 and NSF grant DMS-0510345. The research of E. Tadmor was supported in part by NSF grant 04-07704 and ONR grant N00014-91-J-1076. The research of M. Zhang was supported in part by the Chinese Academy of Sciences grant 2004-1-8.

## References

- [1] P. Arminjon and A. St-Cyr, Nessyahu-Tadmor-type central finite volume methods without predictor for 3d cartesian and unstructured tetrahedral grids, *Appl. Numer. Math.*, 46 (2003), 135-155.
- [2] P. Arminjon, M. C. Viallon, A. Madrane and L. Kaddouri, Discontinuous finite elements and 2-dimensional finite volume versions of the Lax-Friedrichs and Nessyahu-Tadmor difference schemes for compressible flows on unstructured grids, in: M. Hafez and K. Oshima (Eds.), *CFD Review*, John Wiley, 1997, pp. 241-261.
- [3] T. Barth and P. Frederickson, High order solution of the Euler equations on unstructured grids using quadratic reconstruction, *AIAA Paper No. 90-0013*, 1990.

- [4] F. Bianco, G. Puppo and G. Russo, High-order central schemes for hyperbolic systems of conservation laws, *SIAM J. Sci. Comput.*, 21 (1999), 294-322.
- [5] R. Biswas, K. Devine and J. Flaherty, Parallel, adaptive finite element methods for conservation laws, *Appl. Numer. Math.*, 14 (1994), 255-283.
- [6] J. Boris and D. Book, Flux corrected transport I, SHASTA, a fluid transport algorithm that works, *J. Comput. Phys.*, 11 (1973), 38-69.
- [7] N. Chevaugeon, J. Xin, P. Hu, X. Li, D. Cler, J. Flaherty and M. Shephard, Discontinuous Galerkin methods applied to shock and blast problems, *J. Sci. Comput.*, 22/23 (2005), 227-243.
- [8] B. Cockburn and C.-W. Shu, TVB Runge-Kutta local projection discontinuous Galerkin finite element method for conservation laws II, general framework, *Math. Comput.*, 52 (1989), 411-435.
- [9] B. Cockburn and C.-W. Shu, The Runge-Kutta local projection  $p^1$ -discontinuous-Galerkin finite element method for scalar conservation laws, *RAIRO Model. Math. Anal. Numer.*, 25 (1991), 337-361.
- [10] B. Cockburn and C.-W. Shu, The Runge-Kutta discontinuous Galerkin method for conservation laws V: Multidimensional systems, *J. Comput. Phys.*, 141 (1998), 199-224.
- [11] P. Colella and P. Woodward, The piecewise parabolic method (PPM) for gas-dynamical simulation, *J. Comput. Phys.*, 54 (1984), 174-201.
- [12] D. Gottlieb, C.-W. Shu and E. Tadmor, Strong stability-preserving high order time discretization methods, *SIAM Rev.*, 43 (2001), 89-112.
- [13] A. Harten, High resolution schemes for hyperbolic conservation laws, *J. Comput. Phys.*, 49 (1983), 357-393.
- [14] A. Harten, B. Engquist, S. Osher and S. R. Chakravarthy, Uniformly high order accuracy essentially non-oscillatory schemes III, *J. Comput. Phys.*, 71 (1987), 231-303.
- [15] C. Hu and C.-W. Shu, Weighted essentially non-oscillatory schemes on triangular meshes, *J. Comput. Phys.*, 150 (1999), 97-127.
- [16] G.-S. Jiang, D. Levy, C.-T. Lin, S. Osher and E. Tadmor, High-resolution non-oscillatory central schemes with non-staggered grids for hyperbolic conservation laws, *SIAM J. Numer. Anal.*, 35 (1998), 2147.
- [17] G.-S. Jiang and C.-W. Shu, Efficient implementation of weighted ENO schemes, *J. Comput. Phys.*, 126 (1996), 202-228.
- [18] G.-S. Jiang and E. Tadmor, Non-oscillatory central schemes for multidimensional hyperbolic conservation laws, *SIAM J. Sci. Comput.*, 19 (1998), 1892-1917.
- [19] A. Kurganov and D. Levy, A third-order semi-discrete central scheme for conservation laws and convection-diffusion equations, *SIAM J. Sci. Comput.*, 22 (2000), 1461-1488.
- [20] A. Kurganov and C. T. Lin, On the reduction of numerical dissipation in central-upwind schemes, *Commun. Comput. Phys.*, 2 (2007), 141-163.
- [21] A. Kurganov, S. Noelle and G. Petrova, Semidiscrete central-upwind schemes for hyperbolic conservation laws and Hamilton-Jacobi equations, *SIAM J. Sci. Comput.*, 23 (2001), 707-740.
- [22] A. Kurganov and E. Tadmor, New high-resolution central schemes for nonlinear conservation laws and convection-diffusion equations, *J. Comput. Phys.*, 160 (2000), 241-282.
- [23] A. Kurganov and E. Tadmor, Solution of two-dimensional riemann problems for gas dynamics without riemann problem solvers, *Numer. Meth. Part. Diff. Eq.*, 18 (2002), 548-608.
- [24] P. Lax and X.-D. Liu, Solution of two dimensional Riemann problem of gas dynamics by positive schemes, *SIAM J. Sci. Comput.*, 19 (1998), 319-340.
- [25] D. Levy, G. Puppo and G. Russo, A fourth-order central WENO scheme for multidimen-

- sional hyperbolic systems of conservation laws, *SIAM J. Sci. Comput.*, 24 (2002), 480-506.
- [26] X. D. Liu, S. Osher and T. Chan, Weighted essentially non-oscillatory schemes, *J. Comput. Phys.*, 115 (1994), 408-463.
- [27] X.-D. Liu and E. Tadmor, Third order nonoscillatory central scheme for hyperbolic conservation laws, *Numer. Math.*, 79 (1998), 397-425.
- [28] Y. Liu, Central schemes on overlapping cells, *J. Comput. Phys.*, 209 (2005), 82-104.
- [29] Y. Liu, C.-W. Shu, E. Tadmor and M. Zhang, Central discontinuous Galerkin methods on overlapping cells with a non-oscillatory hierarchical reconstruction, *SIAM J. Numer. Anal.*, submitted.
- [30] H. Nessyahu and E. Tadmor, Non-oscillatory central differencing for hyperbolic conservation laws, *J. Comput. Phys.*, 87 (1990), 408-463.
- [31] J. Qiu and C.-W. Shu, On the construction, comparison, and local characteristic decomposition for high-order central WENO schemes, *J. Comput. Phys.*, 183 (2002), 187-209.
- [32] J. Qiu and C.-W. Shu, Hermite WENO schemes and their application as limiters for Runge-Kutta discontinuous galerkin method. II. Two dimensional case., *Comput. Fluids*, 34 (2005), 642-663.
- [33] J. Qiu and C.-W. Shu, Runge-Kutta discontinuous Galerkin method using WENO limiters, *SIAM J. Sci. Comput.*, 26 (2005), 907-929.
- [34] A. M. Rogerson and E. Meiburg, A numerical study of the convergence properties of ENO schemes, *J. Sci. Comput.*, 5 (1990), 151-167.
- [35] R. Sanders and A. Weiser, High resolution staggered mesh approach for nonlinear hyperbolic systems of conservation laws, *J. Comput. Phys.*, 101 (1992), 314-329.
- [36] J. Shi, Y.-T. Zhang and C.-W. Shu, Resolution of high order WENO schemes for complicated flow structures, *J. Comput. Phys.*, 186 (2003), 690-696.
- [37] C.-W. Shu, Numerical experiments on the accuracy of ENO and modified ENO schemes, *J. Sci. Comput.*, 5 (1990), 127-149.
- [38] C.-W. Shu, Essentially non-oscillatory and weighted essentially non-oscillatory schemes for hyperbolic conservation laws, in: A. Quarteroni (Ed.), *Advanced Numerical Approximation of Nonlinear Hyperbolic Equations*, Lecture Notes in Math., Springer, Berlin, vol. 1697, 1998.
- [39] C.-W. Shu and S. Osher, Efficient implementation of essentially non-oscillatory shock-capturing schemes, *J. Comput. Phys.*, 77 (1988), 439-471.
- [40] C.-W. Shu and S. Osher, Efficient implementation of essentially nonoscillatory shock-capturing schemes, II, *J. Comput. Phys.*, 83 (1989), 32-78.
- [41] H.-Z. Tang and T. Tang, Adaptive mesh methods for one- and two-dimensional hyperbolic conservation laws, *SIAM J. Numer. Anal.*, 41 (2003), 487-515.
- [42] B. van Leer, Towards the ultimate conservative difference scheme II. Monotonicity and conservation combined in a second order scheme, *J. Comput. Phys.*, 14 (1974), 361-370.
- [43] P. Woodward and P. Colella, The numerical simulation of two-dimensional fluid flow with strong shocks, *J. Comput. Phys.*, 54 (1984), 115-173.